The *Pseudomonas aeruginosa* T3SS can contribute to traversal of an *in situ* epithelial multilayer independently of the T3SS needle

Eric Jedel [a, b], Daniel Schator [a], Naren G. Kumar [a], Aaron B. Sullivan [a], Arne Rietsch [c], David J. Evans [a, d], Suzanne M. J. Fleiszig [a, b, e #]

a. Herbert Wertheim School of Optometry & Vision Science, University of California, Berkeley, CA USA
b. Graduate Program in Infectious Diseases and Immunity, University of California, Berkeley, CA USA
c. Department of Molecular Biology and Microbiology, Case Western Reserve University, Cleveland, OH USA
d. College of Pharmacy, Touro University California, Vallejo, CA USA
e. Graduate Groups in Vision Science and Microbiology, University of California, Berkeley, CA USA

Running Title: T3SS needle-independent epithelial traversal by *P. aeruginosa*

Corresponding author: Herbert Wertheim School of Optometry & Vision Science, University of California, Berkeley, CA 94720, USA. Tel: +1 (510) 643-0990. Email: fleiszig@berkeley.edu

ABSTRACT

Multilayered epithelia lining our tissue surfaces normally resist traversal by opportunistic bacteria. Previously, we developed a strategy to experimentally perturbate this resistance *in situ* in the corneas of mouse eyes and used it to show that traversal of a multilayered epithelium by *Pseudomonas aeruginosa* requires ExsA, the transcriptional activator of its type 3 secretion system (T3SS). Here, we developed a novel strategy for quantitively localizing individual traversing bacteria within the *in situ* multilayered corneal epithelium and explored contributions of T3SS components. The results showed that T3SS translocon and T3SS effector mutants had reduced epithelial traversal efficiency. Surprisingly, a Δ*pscC* mutant unable to assemble the T3SS needle traversed as efficiently as wild-type *P. aeruginosa*, while a Δ*exsD* mutant 'constitutively on' for T3SS expression was traversal defective. Dispensability of the T3SS needle for effector-mediated traversal was confirmed using a mutant lacking the T3SS operon except the effector genes (Δ*pscU-L* mutant). That mutant reacquired the ability to traverse if complemented with rhamnose-inducible *exsA*, but not if the effector genes were also deleted (Δ*pscU-L*Δ*exoSTY*). Western immunoblot confirmed ExoS in culture supernatants of rhamnose-induced *exsA*-complemented Δ*pscU-L* mutants lacking all T3SS needle protein genes. Together, these results show that epithelial traversal by *P. aeruginosa* can involve T3SS effectors and translocon proteins independently of the T3SS needle previously thought essential for T3SS function. This advances our understanding of *P. aeruginosa* pathogenesis and has relevance to development of therapeutics targeting the T3SS system.

IMPORTANCE

While the capacity to cross an epithelial barrier can be a critical step in bacterial pathogenesis, our understanding of mechanisms involved is derived largely from cell culture experimentation. The latter is due to practical limitations of *in vivo*/*in situ* models and challenge of visualizing individual bacteria in the context of host tissue. Here, factors used by *P. aeruginosa* to traverse an epithelial multilayer *in situ* were studied by: 1) leveraging the transparent properties and superficial location of the cornea, 2) using our established method for enabling bacterial traversal susceptibility, and 3) developing a novel strategy for accurate and quantitative localization of individual traversing bacteria *in situ*. Outcomes showed that T3SS translocon and T3SS effector proteins synergistically contribute to epithelial traversal efficiency independently of the T3SS needle. These findings challenge the assumption that the T3SS needle is essential for T3SS effectors or translocon proteins to contribute to bacterial pathogenesis.

INTRODUCTION

Pseudomonas aeruginosa is a common cause of opportunistic infections, able to cause disease in many body sites including the airways, GI tract, skin, urinary tract, eye, brain, heart and blood (1, 2). Susceptibility can be associated with wounds, burns, immunocompromise, chemotherapy, surgery, predisposing diseases (e.g. cystic fibrosis), and use of indwelling medical devices (3–5). In the eye, *P. aeruginosa* is a leading cause of corneal infection (microbial keratitis), estimated to cause vision loss in approximately 2 million people worldwide each year (6–8). A major risk factor for keratitis is contact lens wear (8–10) and *P. aeruginosa* is the most frequently isolated pathogen from lens-associated infections (6, 10). Recently, an outbreak of multidrug resistant *P. aeruginosa* infections was reportedly transmitted *via* simple artificial tears eyedrops, causing infections of the eye and beyond. These infections resulted in multiple instances of vision loss and several deaths, in some instances without contact lens wear or prior eye disease (11–13).

Type three secretion systems (T3SSs) are among various tools Gram-negative bacteria use to export factors across their otherwise impermeable cell membranes. A T3SS is additionally able to inject effector toxins across host cell membranes into the cytoplasm of a target host cell to alter its biology. *P. aeruginosa* encodes a single T3SS that has been shown to make significant contributions to virulence during acute infections of the cornea (14–17) and other body sites (18–22). The *P. aeruginosa* T3SS is encoded by 42 known genes encoding proteins of a multimeric needle core, a translocon pore, and one or more effector toxins (23). ExsA is the only known transcription factor for these genes. Effectors of the *P. aeruginosa* T3SS, like those of other Gram-negative bacteria, can have a multitude of effects on host cells, including modifying their biology to support an intracellular lifestyle (24–27).

All environment-exposed body surfaces are covered by multilayers of epithelial cells, that when healthy resist traversal by *P. aeruginosa* and other opportunistic bacteria. This includes the cornea of the eye, supremely capable of preventing bacterial colonization through a repertoire of intrinsic defenses, some inherent within the corneal epithelium, others conferred by other factors present at the ocular surface (28–34). The cornea's unique efficacy in this regard makes the corneal surface our only environmentally exposed body surface devoid of a viable bacterial microbiome (35, 36).

If *P. aeruginosa* does adhere to the cornea, which can occur after superficial injury, additional barriers prevent it from traversing the multilayered epithelium to reach the underlying stroma, access to which is required for the initiation of infectious pathology (i.e. keratitis) (28, 37–41). Thus, infection susceptibility requires alterations to the epithelial barrier beyond superficial injury. While that can be accomplished by full thickness injury (42, 43), *P. aeruginosa* corneal infection is most commonly associated with contact lens wear, which predisposes the epithelium to bacterial traversal more subtly by mechanisms not yet well understood (44, 45).

A plethora of studies have been done to explore how *P. aeruginosa* crosses a cultured epithelial cell layer *in vitro*, using a variety of epithelial cell types. For example, airway epithelial cells or MDCK cells were used to show roles for elastase, exotoxin A, type 4 pili, flagella, and the T3SS (46–50). Our own *in vitro* studies using cultured corneal epithelial cells revealed roles for proteases (41), type 4 pilus-associated twitching motility (51), and the T3SS effector ExoU; the latter encoded by only a subset of *P. aeruginosa* strains (cytotoxic strains) and which enables traversal by killing epithelial cells (52). Recently, a study using *in vitro* grown organoids of human airway epithelial cells showed that both the T3SS and type VI secretion system (T6SS) can contribute to *P. aeruginosa* "translocation" (traversal) of an epithelial barrier *via* goblet cell invasion (53).

Thus, our current understanding of how *P. aeruginosa* (and other bacteria) traverse susceptible epithelial layers is based largely on *in vitro* cell culture study outcomes wherein bacteria and host cells are studied in isolation from other factors normally found in their environment *in vivo*. Yet our prior studies have shown that *in vivo* factors modify how bacteria interact with cells, including basement membranes, mucosal fluids, other cell types, nerves, soluble factors, and environmental conditions specific to the tissue site (28, 32, 37, 39, 41, 54, 55). Other limitations of the *in vitro* literature on this topic are that most studies used epithelial cell monolayers that differ from *in vivo* multilayers that contain layers with cells in multiple states of differentiation. Further, transformed cells used by many studies are generally locked into one state of differentiation irrespective of whether they can polarize correctly *in vitro* (e.g. MDCK cells, HeLa cells).

Factors that have hindered development of *in vivo*/*in situ* models for studying epithelial traversal by *P. aeruginosa* and other bacteria include deliberately bypassing epithelial and other tissue barriers to enable infection (e.g. by wounding or bacterial injection through them). Moreover, introducing bacteria *in vivo/in situ* can trigger inflammation that can break down subsequent barriers to bacterial dissemination, reducing or even eliminating the need for bacteria to contribute. Another obstacle to an *in vivo/in situ* study if individual bacteria need to be localized is the challenge of visualizing them in the context of host tissue.

Our published studies have shown that pretreatment of *in vitro* grown corneal epithelial cells with mucosal fluid (tear fluid) increased their resistance to *P. aeruginosa* adhesion, invasion, and cytotoxicity, and increased their traversal resistance when grown as multilayers (39, 56, 57). This was accompanied by profound changes to the epithelial cell's transcriptome (57). Tear fluid exposure also changes gene expression in *P. aeruginosa*, including multiple genes involved in virulence and survival, reducing its ability to traverse cultured corneal epithelial cells - without

directly impacting bacterial viability (39, 57, 58). Other *in vivo* factors that are not present in epithelial cell cultures can modify epithelial-microbe interactions. In the corneal epithelium they include nerves and immune cells, both of which contribute to maintaining epithelial cell homeostasis while also directly recognizing and responding to microbes (28, 31, 32, 59–61). Thus, while cell culture studies have provided a good starting point for understanding epithelial barrier function and mechanisms by which *P. aeruginosa* traverses epithelial cells, *in vivo/in situ* studies are warranted.

Some of our published studies have attempted to address this knowledge gap. In one study, we enabled traversal susceptibility *in vivo* in mice by scratching through the corneal epithelium, then waiting for the time point at which the cell multilayer was reestablished but still remained permissive to bacterial traversal, which occurred 6 hours after scratching (38). Bacterial location and inoculation was quantified in fixed and stained tissue sections. The results showed that mutants lacking ExsA, the transcriptional activator for the T3SS, were unable to traverse the epithelium (38). Since wound healing might have played into the outcome, we later performed a second study enabling susceptibility using more gentle superficial injury, by gently blotting the surface with a KimWipe™, then EGTA-treatment prior to inoculation (37). Using this strategy, we found that bacteria traversing the epithelium did not penetrate past the basal lamina, which when intact functions as a non-specific size exclusion filter (37, 41). This avoids bacterial entry into the stroma and therefore subsequent pathology/inflammation that could complicate studies of how bacteria overcoming epithelial barrier function. In a later study, the blot/EGTA model was used to quantify *P. aeruginosa* traversal of murine corneal epithelium by combining 3D confocal imaging to identify fluorescent bacteria with confocal reflectance microscopy to image the non-fluorescent cornea (62). Results again showed that ExsA was required for *P. aeruginosa* to traverse the corneal

epithelium when the mouse was immunocompetent (62).

A limitation of both of our prior studies was that neither method accounted for the complex shape of the cornea, which is curved rather than flat. The problem this presents is that at any plane of imaging the back and front surfaces of the corneal epithelium are not in line. This made it difficult to accurately determine depth of penetration across the population and ascertain whether T3SS mutants were penetration defective, or simply less efficient at traversing the epithelium.

Here, we report development of an advanced analytical imaging approach allowing for precise metrics of location to be determined for all individual bacteria within the curved multilayered epithelium *in situ*. Use of these methods showed that the T3SS impacts penetration/traversal efficiency of *P. aeruginosa* rather than being absolutely required, with roles played by both the T3SS translocon and T3SS effector proteins. Unexpectedly, results showed that the T3SS needle was dispensable for this phenotype, and actually interfered when constitutively expressed.

RESULTS

Transcription of the T3SS promotes *P. aeruginosa* traversal efficiency in the multilayered corneal epithelium *in situ*. Our prior study showed that the transcriptional activator of the T3SS (ExsA) contributed to *P. aeruginosa* traversal of the mouse eye's corneal epithelium (62). Here, we leveraged recent advances in imaging and image analysis to obtain more detail about how ExsA impacts bacterial location, taking into account the complexities of the cornea's shape while more accurately assessing location of individual members of the traversing population.

As in our previous study, we used confocal reflectance microscopy (CRM) to image the corneal epithelium and GFP-expression to detect bacteria. Raw confocal images were then imported into

Imaris software v9.9 for processing, the CRM signal pseudo-colored red (Fig. 1A). As detailed in the methods section, the reflectance signal from the stroma was manually excluded, and a "Surface" representing only signal from the epithelium was generated (Fig. 1B). Apical and basal boundaries of the epithelium were then identified (Fig. 1C). Individual bacteria were identified as a "Spot", creating objects in the image that each represented one population member (Fig. 1D). The distance (in microns) from the apical and basal boundary of the epithelium was measured for each bacterial "Spot", and the depth of penetration of each bacterium was calculated as a percentage to provide its relative position in between the upper and lower epithelial boundaries, with 0% being surface adherent and 100% meaning that the bacterium reached the underlying basal lamina (Fig. 1E). Another metric quantified was the proportion of the population able to penetrate beyond the 50% (midpoint) normalized to the thickness of the epithelium in that region of the tissue (as in Fig. 2B).

The first experiment was conducted using *P. aeruginosa* strain PAO1F wild-type compared to an isogenic Δ*exsA* mutant: corneas were incubated with 600 µl of ~10^{11} CFU/ml bacteria for 6 h (see Methods). The goal was to compare the outcome to our prior study that used more rudimentary methods. For wild-type, the median traversal depth of individual bacteria was 47.29% of the epithelial thickness, the upper quartile reaching at least 76.02% depth (Fig. 2A). Fig. 2B shows that 47.27% of the bacterial population penetrated beyond 50% thickness of the epithelium. In contrast, median penetration depth for Δ*exsA* mutant was only 7.31% depth, the upper quartile being at only 12.86% depth (Fig. 2A). Only 2.67% penetrated beyond the midway point (50% depth) (Fig. 2B). While these findings confirmed the importance of the T3SS in corneal epithelial traversal by *P. aeruginosa* shown in our earlier publications, they provided more granularity on how it impacts bacterial location/distribution. The pattern that emerged showed that the *exsA*

mutants lacking the entire T3SS were not completely defective in ability to penetrate beyond the epithelial surface, with significant variability among the population. While wild-type penetrated more deeply than T3SS mutants over the 6 h time span of these experiments, there was again significant variability with only a fraction fully traversing to the level of the underlying basal lamina. For this reason, the capacity to penetrate the corneal epithelium is referred to as traversal efficiency for the remainder of this manuscript.

Efficient traversal involves T3SS effectors and the T3SS translocon but does not require the T3SS needle apparatus. To explore which ExsA-regulated T3SS components are required for traversal efficiency, we compared wild-type *P. aeruginosa* to mutants lacking the T3SS needle apparatus (Δ*pscC*), the T3SS effectors (Δ*exoSTY*), or the T3SS translocon proteins (Δ*popBD*).

As shown in Fig. 2A, both the T3SS effector mutants (Δ*exoSTY*) and the T3SS translocon mutants (Δ*popBD*) were defective in traversal efficiency compared to wild-type reaching median traversal depths of 11.16% and 10.91% respectively, comparable to the Δ*exsA* mutant. Compared to the Δ*exsA* mutant, a greater proportion of the Δ*popBD* or Δ*exoSTY* mutant populations traversed to over 50% depth; 30.18% and 19.27% respectively (Fig. 2B). Surprisingly, the Δ*pscC* mutant lacking the T3SS needle, was the most traversal efficient of all of the mutants examined, with median traversal at 45.24% depth, similar to wild-type.

These outcomes were surprising given that the T3SS needle is considered important for T3SS functions. Thus, we additionally tested a Δ*exsD* mutant that is constitutively active for the T3SS and therefore consistently expresses T3SS components (including the needle). This differs from wild-type which instead requires induction by host cell contact or low calcium to express the T3SS, and it is effectively the opposite of a Δ*exsA* mutant which consistently lacks T3SS expression.

Results with the Δ*exsD* mutant showed that constitutive expression of the T3SS actually interferes with traversal efficiency, showing a median traversal depth of only 12.66% (Fig. 2A), with only 21.42% of the population penetrating beyond 50% depth (Fig. 2B). Representative examples of epithelium traversal by wild-type bacteria and T3SS mutants are shown in Supplemental Fig. S1.

Since traversal efficiency data within these different populations was not normally distributed, the Kruskal-Wallis test with Dunn's multiple comparisons was used to compare each mutant to the Δ*exsA* mutant. Due to the very large sample sizes (10,000-60,000 datapoints each group), all comparisons were found to be highly statistically significant ($P < 0.0001$), even when median values and distributions appeared visually comparable (Fig. 2A). This was also true when comparing mutants to wild-type. For this reason, the magnitude and the direction of the differences are important to consider in evaluating the biological significance of the outcomes. Taking those parameters into consideration, the data showed that traversal efficiency was supported by combined efforts of the T3SS effectors and the T3SS translocon. They further suggested that the T3SS needle was not required, and that constitutively expressing it and other T3SS factors in the entire population actually detracted from traversal efficiency. Since this result was unexpected, we used Sanger sequencing to re-confirm that the Δ*pscC* mutant used contained a clean deletion of *pscC* (data not shown). In other controls, the T3SS-GFP reporter pJNE05 (P_{exoS} expression) was used to confirm that P_{exoS} was activated upon EGTA-exposure similarly to wild-type in each of the mutants shown to be defective in traversal in Fig. 2: Δ*popBD*, Δ*exoSTY* and Δ*exsD* (Supplemental Fig. S2). Since P_{exoS} expression is a reliable surrogate for *exsA* expression, this outcome confirmed that the mutants were not defective for T3SS induction, at least under the conditions used.

Complementation of ExsA in the Δ*pscU-L* T3SS operon mutant restored T3SS effector-

dependent traversal efficiency. The above results using T3SS needle mutants and constitutive expression of the T3SS showed that the capacity to make the T3SS needle did not correlate with efficient traversal despite involvement of the T3SS effectors. Here, we directly tested the hypothesis that the effectors can function without the needle.

First, we generated a mutant lacking the 36 genes in the main T3SS operons, from Δ*pscU* to Δ*pscL* (designated Δ*pscU-L*). This mutant still encodes the known T3SS effectors in PAO1 (ExoS, ExoT and ExoY) and their chaperones under endogenous promoters. Results showed the Δ*pscU-L* mutant had low traversal efficiency (Fig. 3A, B) thereby phenocopying the Δ*exsA* mutant. This was to be expected since the Δ*pscU-L* mutant lacks the gene encoding ExsA in addition to genes encoding all of the T3SS machinery proteins, and while it does encode the T3SS effectors, these are not transcribed, translated or released without ExsA.

Next, we tested if expressing the T3SS effectors in this mutant lacking T3SS machinery related proteins could rescue traversal efficiency. This was done by complementing the mutant with ExsA using a chromosome-integrating vector to induce expression of *exsA* under a rhamnose-sensitive promoter. This vector was first tested in the background of a Δ*exsA* mutant using a GFP reporter pJNE05 for P_{exoS} expression as a surrogate for *exsA* induction (as above, Supplemental Fig. S2). Rhamnose addition induced GFP expression and it significantly increased bacterial traversal compared to the no rhamnose control for the Δ*exsA*:P_{rha}*exsA* mutant (Supplemental Fig. S3A, B). We next showed that Rhamnose-induction of *exsA* expression in the Δ*pscU-L* mutant background increased median traversal to 11.09% depth versus the rhamnose-induced vector control at 7.34% depth (Fig. 3A), and it also increased the percentage of the population that traversed to at least 50% depth to 18.35% vs. 0.00 % (Fig. 3B). Showing that partial restoration of traversal efficiency by Δ*pscU-L*:P_{rha}*exsA* depended on the T3SS effectors, it was abrogated when the three exotoxin

277 genes were also deleted (Median: 5.76% depth, population over halfway 0.00%) (Fig. 3A, B). An
278 *in vitro* control with pJNE05 confirmed activation of P_{exoS} in the Δ*pscU-L* mutant after *exsA*
279 complementation with rhamnose addition relative to a vector-complemented control: Mean +/- SD
280 P_{exoS} expression (FITC/OD_{600}) for Δ*pscU-L*:P_{rha}*exsA* + rhamnose was 3397 ± 1033 relative
281 fluorescence units versus 1567 ± 1235 for Δ*pscU-L*:P_{rha}Vector + rhamnose (P = 0.0061, Student's
282 t-Test).

283 In Fig. 3A all comparisons between groups were significant (P < 0.0001 for most comparisons,
284 and P = 0.025 comparing Δ*pscU-L* [no rhamnose] *vs.* Δ*pscU-L*Δ*exoSTY*:P_{rha}*exsA* [+ rhamnose],
285 Kruskal-Wallis test with Dunn's multiple comparisons). The latter comparison compared two
286 mutants both unable to express T3SS effectors or any of the T3SS machinery-related proteins, only
287 one able to express the transcriptional activator ExsA (Fig. 3A, B). Thus, ExsA expression in the
288 absence of those other components had the least impact on traversal efficiency. Taken together,
289 these results show that ExsA-driven expression of *exoSTY* can increase traversal efficiency of a
290 mutant lacking all the T3SS machinery and thus one or more effectors are necessary for traversal.
291 However, it remains possible that ExsA regulates the expression of a factor(s) outside of the main
292 T3SS operon that is/are needed for effector-mediated traversal.
293
294 **The T3SS translocon contributes to traversal efficiency beyond roles of the T3SS effectors,**
295 **also independently of the T3SS needle.** To explore if the T3SS translocon contributes to traversal
296 efficiency beyond the impact of the T3SS effectors, we studied deletion of *popB* in the background
297 of a Δ*exoSTY* mutant (already reduced in traversal efficiency compared to wild-type). This led to
298 a small but statistically significant further reduction in median traversal depth: Δ*exoSTY* median
299 at 10.91% depth vs. Δ*popB*Δ*exoSTY* median at 8.10% depth (Fig. 4A, Δ*exoSTY* data reproduced

from Fig. 2) ($P < 0.0001$, Kruskal-Wallis test with Dunn's multiple comparisons). A much bigger reduction was seen in the percent of population traversing beyond the 50% point: Δ*exoSTY* 19.27% vs. Δ*popB*Δ*exoSTY* 1.62%.

We next tried the opposite experiment, deleting a T3SS effector gene (*exoS*) in a T3SS translocon mutant (*popB*). This also showed separable contributions for the T3SS effectors and the T3SS translocon, the median depth for a Δ*popB* mutant at 12.30% depth vs. median for Δ*popB*Δ*exoS* mutants at 9.42% depth (Fig. 4A) ($P < 0.0001$, Kruskal-Wallis test with Dunn's multiple comparisons). Again, the difference became more obvious when assessing the percent of the population penetrating beyond 50% depth; Δ*popB* 17.76% vs. Δ*popB*Δ*exoS* 5.86% (Fig. 4B). Taken together, these results showed that T3SS translocon proteins and T3SS effector proteins can have additive impacts on traversal efficiency and specifically implicate ExoS and PopB. However, difference in traversal beyond 50% depth shown between Δ*popB*Δ*exoS* 5.86% and Δ*popB*Δ*exoSTY* 1.62% implicate a role(s) for ExoT and/or ExoY.

Having already shown that the T3SS needle was dispensable for effector mediated traversal, we next asked if it was needed for the translocon's contribution. Thus, we mutated the translocon pore proteins PopB and PopD (Δ*popBD* mutant) in the background of the T3SS needle mutant (Δ*pscC*) already shown to be traversal competent (Fig. 2). This reduced traversal efficiency of the needle mutant: Δ*pscC* mutant median 45.24% depth, population over halfway 43.84% vs. Δ*pscC*Δ*popBD* mutant median at 36.11% depth, population over halfway at 35.00% (Fig. 4A, B, Δ*pscC* data reproduced from Fig. 2) ($P < 0.0001$, Kruskal-Wallis test with Dunn's multiple comparisons). This showed that the T3SS translocon can contribute to traversal efficiency in the absence of the T3SS needle.

All traversal results and strain characteristics are summarized in Table 1. Together, these

outcomes implicate two separate contributors to T3SS-mediated traversal efficiency: the T3SS effectors (including ExoS), and the T3SS translocon pore (including PopB), each functioning independently of the T3SS needle which can instead play an inhibitory role. Interestingly, the magnitude of their individual contributions appear similar in magnitude, the Δ*exoSTY* and Δ*popB* mutants showing no significant difference in impact (Fig. 4).

Exotoxin S protein can be released by a T3SS operon mutant. Results in Figs. 2-4 show that the T3SS effectors can contribute to traversal efficiency without the T3SS needle genes. Our current understanding of T3SS transcription and expression is that in the presence of Ca^{2+} or absence of host cell contact, low levels of T3SS expression occur due to repression of ExsA by ExsD (63). Upon host cell contact or Ca^{2+} deprivation, the T3SS regulator ExsE is secreted, leading to ExsA de-repression and T3SS transcription. *In vitro*, Δ*pscC* needle mutants do not secrete ExsE and do not activate high levels of T3SS expression (64). To test if an alternate mechanism of T3SS effector toxin expression might be operating in our *ex vivo* traversal model or T3SS mutants, the Δ*exsA* or Δ*pscU-L* mutant carrying rhamnose-inducible *exsA* were tested for ExoS protein expression *in vitro* using LB broth without EGTA calcium chelation to specifically test rhamnose induction compared to controls (vector only or no rhamnose). After growth in broth culture to 'mid-log' phase, bacterial pellet and supernatant samples were collected and probed for ExoS *via* affinity-purified polyclonal antibody using SDS-PAGE and Western immunoblot as described previously (64). ExoS protein was detected in the pellet and supernatant of Δ*exsA*:P_{rha}*exsA* with rhamnose induction (as expected) and in Δ*pscU-L*:P_{rha}*exsA* with inclusion of rhamnose but not in its vector control (Fig. 5). These data confirmed that ExsA-driven ExoS expression and release can occur for mutants lacking needle protein genes.

DISCUSSION

Previously, we showed that the transcriptional activator of the T3SS (ExsA) is required for *P. aeruginosa* to traverse susceptible multilayered epithelium in the context of live tissue, shown using the eyes of immunocompetent mice (38, 62). Here, we explored the role of T3SS components.

The cornea has several advantages over other tissues for this type of investigation being readily accessible for manipulation or imaging, optically clear when healthy allowing imaging without 2-photon microscopy or tissue clearing protocols and is relatively separated from other body sites reducing complexity associated with cross-talk that can occur during infection. Its epithelial surface also lacks a microbiome (35, 36), allowing a pathogen to be studied alone or in combination with other bacteria in a controlled fashion. Use of subtle epithelial injury to enable susceptibility to bacterial traversal, as done in this study using tissue paper blotting then EGTA treatment, preserves the underlying basal lamina barrier, prohibiting bacterial access to the vulnerable stroma and allowing study of epithelial traversal by bacteria without complexities introduced by later steps of infection development. Thus, this mouse eye model for studying epithelial traversal shares some advantages of *in vitro* cell/tissue culture models in reducing complexity but benefits from *in situ* context.

A challenge of *in situ* tissue imaging for quantitively localizing bacteria is variations in tissue shape that can make it difficult to ascertain position relative to upper and lower boundaries across an entire tissue sample. Here, we developed methods that account for the cornea's curved surface, variations in thickness and topography in different regions and resulting from cell exfoliation, and

any changes to these parameters after exposure to bacteria. This allowed for more precise quantitation of bacterial location between the epithelial surface and underlying basal lamina, separately accounting for all individual bacteria present in the epithelial layer.

To calibrate outcomes to our previously published methods, we first compared wild-type *P. aeruginosa* to mutants lacking the entire T3SS *(exsA* mutants) which confirmed the critical role for the T3SS in corneal epithelium traversal. However, the more accurate localization method showed traversal was not an absolute quality, with both wild-type *P. aeruginosa* and *exsA* mutants showing a distribution/spread for individual bacteria in their penetration rates. Thus, we referred to "traversal efficiency" rather than "traversal" to describe subsequent outcomes.

When roles of specific T3SS components were examined, some results aligned with *in vitro* cell culture study findings (65). For example, mutants lacking genes for known T3SS exotoxins had reduced traversal efficacy compared to wild-type. However, our study showed that mutants in T3SS translocon pore proteins also showed reduced traversal efficiency, with mutants lacking both translocon and exotoxin proteins showing an even more profound defect similar to *exsA* mutants unable to express any T3SS components. This implicated both the T3SS effectors and the T3SS translocon proteins, their roles being additive.

Not all outcomes aligned with *in vitro* study findings. Mutants lacking the T3SS needle were just as traversal efficient as wild-type *in situ.* This was a surprising and confusing result because the T3SS needle is generally thought critical for T3SS function, including for secretion or expression of the very same T3SS components we found required for traversal efficiency. Thus, we used a mutant lacking the entire T3SS operon except the genes encoding the effector exotoxins (Δ*pscU-L* mutant) (66) and induced effector expression by complemented it with rhamnose inducible *exsA* (the transcriptional activator of all T3SS-related genes). This promoted traversal

efficiency in the mutant despite it lacking T3SS needle and other machinery related proteins. Confirming it was T3SS effector gene expression driving the phenotype in the T3SS operon mutant not than other genes outside the T3SS operon, traversal was no longer promoted by *exsA* complementation when the effector genes were also mutated (i.e. Δ*pscU-L exoSTY* mutant). Since Δ*pscU-L* mutants lack T3SS translocon genes additionally needed for full traversal efficiency, it was not surprising that *exsA* complementation did not fully restore the operon mutant to wild-type traversal efficiency. Indeed, efficiency approximated translocon (*popBD*) mutants that similarly encode T3SS effectors but not translocon proteins, but that differ in encoding T3SS needle proteins. Together these results confirmed that the T3SS needle protein genes are not needed for T3SS effector-mediated traversal efficiency in this *in situ* model.

Since T3SS needle proteins are thought necessary for exporting T3SS effectors out of bacteria and for injecting them into host cells this data raised two related questions. Can T3SS effectors become extracellular without the needle, and if so, how do they impact traversal without being injected into host cells?

Western immunoblotting confirmed the presence of ExoS in both supernatant and pellet of *in vitro* grown Δ*pscU-L*:P_{rha}-*exsA* after rhamnose induction, showing that ExoS can become extracellular without needle protein genes. While this might be an unusual feature of this mutant, that would not explain results with other mutants that also show the needle is dispensable for T3SS mediated traversal efficiency. A potential explanation is that bacterial lytic cell death releases effectors, e.g. explosive cell lysis in *P. aeruginosa* (67), and a feature of other toxin release by other bacteria (68, 69) and quite possible given the dense bacterial inoculum and routine 'natural' bacterial cell death as a result of nutrient deprivation or from formation of biofilms (67). In the context of our *in situ* assay, the presence of host-derived antimicrobial peptides (29, 33, 70) could

415 further contribute to bacterial cell death. Alternatively, T3SS proteins are packaged into OMVs
416 (Outer Membrane Vesicles) that are released into the extracellular environment, as shown for
417 *Salmonella enterica* T3SS-1 effectors and translocation proteins (71). Indeed, some T3SS proteins
418 were efficiently secreted *via* OMVs by mutants lacking a functional T3SS needle, and effector
419 toxins were shown delivered *via* OMVs into the cytoplasm of epithelial cells where they enhanced
420 pathogenesis of T3SS-deficient mutants (72). Pathogenic *E. coli* (O157:H7) can also efficiently
421 package T3SS translocation and effector proteins into OMVs in the absence of essential T3SS
422 needle proteins (73). Our own work showed that exposing *P. aeruginosa* to ocular surface tear
423 fluid or to purified lysozyme (a tear fluid ingredient) generates OMVs that are cytotoxic to the
424 corneal epithelium of mouse eyes *in vivo*. We also showed that priming the corneal surface with
425 these OMVs reduces defense against bacterial adhesion, and that tear fluid/lysozyme triggered
426 OMVs contain a ~48 kDa protein similar in size to ExoS (~49 kDa) and ExoT (~53 kDa) (74).
427 Another potential pathway for delivering T3SS effectors into a host cell without the T3SS needle
428 could be from an intracellular location. In this regard, it is interesting that the results specifically
429 implicated PopB and ExoS in traversal efficiency as our work has shown critical roles for both in
430 the intracellular lifestyle of *P. aeruginosa* (24–27, 75). Notwithstanding, even T3SS mutants are
431 internalized by epithelial cells and can persist inside intracellular vacuoles that can subsequently
432 fail to contain them (24–26, 75–78). In other words, T3SS factors can facilitate but are not essential
433 for bacterial entry into a host cell's cytoplasm. Inside epithelial or other cells, bacteria (including
434 *P. aeruginosa*) can use factors beyond T3SS factors to exert impacts on the host cell, and the host
435 cell can detect intracellular bacteria and in response alter its biology and/or induce programmed
436 cell death. Others have shown that extracellular ExoS itself can be internalized by eukaryotic cells,
437 and activates host cell TNF-α responses by triggering surface TLRs (79). While mechanisms might

438 overlap with some of the above, ExoS has also been shown to affect host cell function from an
439 extracellular location (80).

440 Given these many possibilities, a separate study will be needed to determine how T3SS effector
441 mediated traversal occurs without the T3SS needle. Importantly, much of our understanding of
442 gene expression in *P. aeruginosa* has been done using *in vitro* methods, often without host cells
443 present. Given its many environmental sensors and regulators of gene expression, regulation of the
444 *P. aeruginosa* T3SS *in situ/in vivo* could differ vastly from what has been shown *in vitro*. It is also
445 likely to be context dependent/complex due to microenvironments, and lack of homogeneity and
446 synchrony. Indeed, the result showing that *exsD* mutants (which differ from wild-type in
447 constitutively expressing the T3SS) are equally as traversal defective as mutants lacking the entire
448 T3SS are particularly poignant and highlight the importance of regulation. Further research on this
449 topic would benefit from more *in situ* experimentation to set the stage for well-designed *in vitro*
450 studies that can then tease apart mechanisms for the phenomena shown relevant to pathogenesis
451 *in situ/in vivo*.

452 The T3SS translocon proteins (PopB/PopD) were found to play roles additional to the
453 contribution of the effectors. This could relate to their ability to form pores in host cell membranes,
454 which can damage a cell or otherwise alter host cell function. Indeed, PopB-PopD complexes in
455 isolation have been shown to function as a pore-forming toxin by allowing K^+ efflux, resulting in
456 histone H3 modification and host cell subversion (81). A potential mechanism for the additive
457 impacts of translocon and effector proteins could be pore formation providing an entry mechanism
458 for effector delivery into the host cell. Whether the T3SS needle is also dispensable for translocon-
459 mediated traversal efficiency remains an open question that will require further investigation,
460 although it is suggested by the fact that needle mutants remain fully efficient.

Another factor to consider in interpreting the data is that T3SS needle proteins of *P. aeruginosa* and other Gram-negative bacteria are recognized by mouse (and human) cells causing inflammasome activation (82, 83), which can help the cornea and other tissues recognize, respond and clear *P. aeruginosa* during experimental challenge *in situ* (35, 84). In this way, expressing T3SS needle proteins could be detrimental to bacteria *in situ* (even if not *in vitro*) and using needle-independent mechanism for traversal could be advantageous. Other *in situ* factors (absent *in vitro*) may also impact bacterial viability or growth during traversal and thus data interpretation.

Providing additional insights into pathogenesis, traversing bacteria tended to be bimodally distributed across the epithelium. Typically, there was a cluster in the apical region from 0-15% traversed, few across the midway point, then a group from 50-80% traversed. This distribution may reflect bistability of T3SS expression in *P. aeruginosa* populations (26, 85), and/or a host defense barrier, possibly related to specialized junctions in the suprabasal region of the corneal epithelium that have been shown to be a barrier to leukocytes (86). Also worth noting, the very large sample sizes (10,000-60,000 datapoints for each group) provided such a powerful analysis, that most comparisons yielded statistically significant differences even when they were small. Thus, we considered the magnitude of the differences in central tendency (median) and data spread (upper and lower quartiles) to draw conclusions about biological significance.

In conclusion, this study used novel and powerful image analysis tools and an *in situ* model with pared-down complexity to focus on an early step in pathogenesis, traversal of a superficial multilayered epithelium. The goal was to determine which T3SS components contribute. Results showed roles for T3SS effectors, T3SS translocon proteins, and regulation of T3SS expression. Differing from *in vitro* culture studies and challenging our general understanding about how the *P. aeruginosa* T3SS supports infection pathogenesis, the T3SS needle was dispensable. Follow up

484 experiments confirmed that the T3SS effector ExoS could become extracellular in the absence of
485 the T3SS needle. How T3SS effectors and translocon proteins influence host cells to promote
486 traversal without the T3SS needle will require further work. Published knowledge about *P.*
487 *aeruginosa* and other Gram-negative bacteria suggest multiple possibilities (67, 72, 73, 87).

488 Outcomes of this study may or may not be applicable to how *P. aeruginosa* traverses epithelial
489 barriers other than the mouse corneal epithelium, but if so they might generally inform efforts to
490 develop therapies targeting the T3SS (88, 89). Importantly, the results highlight the need to move
491 beyond *in vitro* and cell culture studies when studying pathogenesis. At the same time, they support
492 complementary *in vitro* and cell culture experimentation that can further reduce complexity when
493 teasing apart details, and to study regulation in a more controlled system.

494 The model and imaging methods we have developed enable a single early stage of infection
495 pathogenesis to be studied *in situ* in the absence of various confounders generally present in
496 infection models (e.g. inflammation), and they enable individual bacteria to be visualized across
497 the entire tissue with their location quantified. These methods could prove useful for studying
498 pathogenic strategies of other microbes also able to traverse epithelial layers during infection,
499 including those not considered to be eye pathogens.

500

501 **MATERIALS AND METHODS**

502

503 **Bacteria.** *Pseudomonas aeruginosa* strain PAO1F was used for all experiments. Mutants in T3SS
504 components were either obtained from in-house strain collections or generated using two-step
505 allelic exchange (90). For this, pEXG2 vectors containing overlapping upstream and downstream
506 regions of the genes of interest (excluding the ORF) were cloned and transformed to *E. coli* SM10

(λ*pir*), which were then used as donor strains to deliver the vector to recipient *P. aeruginosa* strains. Successful merodiploid colonies underwent sucrose counter-selection and PCR verification of mutagenesis. For integration of rhamnose-inducible ExsA, Dr. Arne Rietsch provided strains generated by Tn7 vector-mediated insertion and Flp-mediated excision of antibiotic resistance markers (91). All bacteria, mutants and plasmids used are shown in Table 2. In control experiments not shown, T3SS mutants did not show any growth defects relative to PAO1 in trypticase soy broth culture at 37 ºC *in vitro*.

For all experiments, bacteria were streaked from glycerol stocks stored at -80 ºC, plated onto trypticase soy agar (TSA) plates with appropriate antibiotics (see Table 2) and grown at 37 ºC overnight. For the rhamnose-induction traversal experiments, bacteria were grown on TSA also supplemented with rhamnose (2 %). For T3SS-induction growth curves with plasmid pJNE05, bacteria were grown in trypticase soy broth (TSB) supplemented with gentamicin (200 μg/ml), monosodium glutamate (100 mM), glycerol (1%) and EGTA (2 mM) or alternatively with rhamnose (2 %) instead of EGTA as specified.

For the *ex vivo* murine model of traversal, one bacterial "lawn-covered" TSA plate was used per bacterial strain per condition. After overnight growth at 37 ºC, bacteria were collected with a sterile loop and carefully suspended into serum-free DMEM (Dulbecco's Modified Eagle medium; Gibco). DMEM was supplemented with 2% rhamnose when indicated. OD_{600} was measured, with A_{600} 1.0 ~ 4 x 10^8 CFU/ml used for calculating density. Suspensions of 1.0 x 10^{11} CFU/ml were used for *ex vivo* incubations, and concentrations confirmed by plating serial dilutions for viable counts.

***Ex vivo* murine model of traversal.** All procedures were approved by the Animal Care and Use

Committee of the University of California, Berkeley, an AAALAC accredited institution. For all experiments, male or female C57BL6/J or mT/mG mice with tdTomato-labeled cell membranes were used, 6 to 12 weeks old, and 3-6 eyes per experimental condition. Contralateral eyes from the same mouse were used as controls when possible. All experiments were performed *ex vivo*, as mice were euthanized by isoflurane inhalation prior to any further manipulations. After euthanasia, each eye was lightly blotted with a Kimwipe (Kimtech), enucleated, then placed in 0.2µm filter-sterilized 1X Phosphate-Buffered Saline (PBS) in a 48-well dish for subsequent steps. Eyes were rinsed three times in PBS, then incubated in a 0.1M solution of EGTA at room temperature for 1 h. Eyes were rinsed three more times in PBS, then completely submerged in a 600 µl suspension of bacteria, prepared as described above, and incubated at 37 ºC, 5 % CO_2 for 6 h, consistent with our previous studies (62, 92). Following this incubation, eyes were rinsed with PBS three times to remove excess non-adherent bacteria before fixation in 2 % paraformaldehyde (PFA) overnight at 4 ºC. Fixed eyes were then whole mounted on a glass cover slip with Loctite superglue with the central cornea facing up before submersion in PBS and imaging.

Imaging. Whole-mounted fixed corneas were imaged using an Olympus Fluoview FV1000 upright laser scanning confocal microscope with a water immersion 20X objective (NA = 1.0). For each eye, three to five non-intersecting fields of view on the central cornea were selected for imaging with 3x optical zoom (60x total magnification) at 1024 x 1024 resolution and 0.8µm step size. Fluorescent bacteria were imaged using FITC (488/509) and/or RFP (555/580) channels, and corneal cells were imaged using an 640nm excitation channel for confocal reflectance microscopy (CRM) (92, 93).

Image analysis. Images of corneas were processed on Imaris Software (v 9.9) as follows. First, a "surface object" was manually drawn using the reflectance channel to select the total signal underneath the corneal basement membrane. This object represented the corneal stroma and was used to mask the remaining reflectance signal. This created a new channel with signal from only the epithelium, which was used to automatically generate a new surface object.

From the created Epithelium surface object, a distance transformation was performed, and the basement membrane and apical surface were identified as two new surface objects ~1µm away from the Epithelium. Variability in the created objects due to differing corneal reflectance intensity was minimized through use of automatic thresholds, and manual surveillance of the entire process ensured consistency in appearances. Next, bacteria were identified through the 'Spots' tool, using an XY size of 1.25 µm in the appropriate channel. Parameters for Spots creation were assessed using an automatic threshold, adjusted manually to reduce false positive results (e.g., Spots where there were no bacteria).

For each field of view, the following were measured: total volume and maximum thickness of epithelium, total number of bacteria, and distance of each bacterium from apical surface and basement membrane. Percent depth of traversal for each bacterium was calculated using the formula: % Depth = Distance to Apical Surface / (Distance to Apical + Distance to Basement Membrane) * 100 %. An inverted cumulative histogram was also generated from the % depth for all bacteria in a condition with 5µm bins. The percent of the total population remaining deeper was graphed, so 100 % of a population remained at 0 % traversal depth and 0 % remained at 100 % depth.

Western immunoblot. Bacteria were inoculated in liquid cultures of LB media (containing 200

mM NaCl, supplemented with 10 mM $MgCl_2$) and grown with shaking overnight at 37 ºC. Overnight cultures were diluted 1:300 into fresh media, grown for 2 h, then 1 ml of culture was added to 1 ml pre-warmed media with 2 % rhamnose and 1 ml of culture was added to 1 ml pre-warmed media as a control. The bacteria were grown for another hour before the OD_{600} was measured for each tube, which were then placed on ice. 1 ml of each sample was pelleted, and the entire supernatant was added to a fresh tube containing 10 % trichloroacetic acid for precipitation. After 10 min on ice, two washes with acetone were conducted before drying out the precipitate at room temperature. The cell pellet and supernatant precipitate were both resuspended in the same volume of 1x SDS Buffer (Laemmli Solution [Bio-Rad], 1 mM DTT) to create a concentration of 4 x 10^9 CFU/ml, or an OD_{600} of 10 – typically 60-80 µl. Samples were boiled at 90 ºC for 10 min to denature proteins before brief centrifugation.

For SDS-PAGE, 50 µl of each sample and Precision Plus Protein Standards (Bio-Rad) were then applied to a 4-20 % Protean TGX Stain Free Gel (Bio-Rad) before separation at 200V for 35 min. Gels were imaged on the Bio-Rad Gel Dock, then transferred to nitrocellulose membranes using the Mixed MW program on the TransBlot Turbo Transfer System. Membranes were blocked with EveryBlot buffer (Bio-Rad) before incubation overnight at 4 ºC with an affinity-purified Rabbit polyclonal anti-ExoS primary antibody (from Dr. Arne Rietsch, 1:5000). After washing 3x with TBS-T (0.1 % Tween-20 in 1x TBS Buffer) for 5 min each, membranes were then incubated for 1 h at RT with Goat anti-Rabbit HRP-conjugated secondary antibody (ThermoFisher A16096, 1:1000). Membranes were again washed with TBS-T, then exposed to Clarity Western ECL substrate (Bio-Rad) for 5 min before chemiluminescence and colorimetric imaging.

Statistical analysis. Data on bacterial depth from Imaris were exported into Microsoft Excel and

599 GraphPad Prism 9 or 10 for visualization and analysis. The percent depth for each individual
600 bacterium was considered a unique data point and were aggregated across all fields of view for
601 each eye as one biological replicate. Data from 3-6 biological replicates for each condition were
602 combined into a single column for graphing and shown as median ± interquartile range. For all *ex*
603 *vivo* experiments, data did not pass normal distribution tests. The Kruskal-Wallis test with Dunn's
604 multiple comparisons or Kolmogorov-Smirnov test were used to compare groups. For growth
605 curve comparisons, One-way ANOVA with Dunnett's multiple comparisons or a paired Student's
606 t-Test were used. $P < 0.05$ was considered significant.
607
608 **Funding Information.** This work was supported by the National Institutes of Health; R01
609 EY011221 (SMJF) and R21 AI180421 (AR). The funding agency had no role in study design, data
610 collection and interpretation, or decision to publish.
611
612 **Acknowledgements.** Thanks to Dr. Alain Filloux (Imperial College London, UK) for originally
613 providing *P. aeruginosa* wild-type strain PAO1F.
614
615 **Contributions.** EJ, DS, NGK, AR, DE and SF designed the experiments; EJ, DS, NGK and AR
616 performed the experiments; EJ, AR, AS, DS, NGK, DE and SF analyzed and interpreted the data;
617 EJ, DE, AR and SF wrote the manuscript; DE and SF supervised the study.

REFERENCES

1. Morin CD, Déziel E, Gauthier J, Levesque RC, Lau GW. 2021. An organ system-based synopsis of *Pseudomonas aeruginosa* virulence. *Virulence* 12:1469-1507

2. Juan C, Peña C, Oliver A. 2017. Host and pathogen biomarkers for severe *Pseudomonas aeruginosa* infections. *J Infect Dis* 215:S44–S51.

3. Vincent JL, Sakr Y, Singer M, Martin-Loeches I, MacHado FR, Marshall JC, Finfer S, Pelosi P, Brazzi L, Aditianingsih D, Timsit JF, Du B, Wittebole X, MácA J, Kannan S, Gorordo-Delsol LA, De Waele JJ, Mehta Y, Bonten MJM, Khanna AK, Kollef M, Human M, Angus DC. 2020. Prevalence and outcomes of infection among patients in intensive care units in 2017. *JAMA* 323:1478-1487.

4. Magill SS, Edwards JR, Bamberg W, Beldavs ZG, Dumyati G, Kainer MA, Lynfield R, Maloney M, McAllister-Hollod L, Nadle J, Ray SM, Thompson DL, Wilson LE, Fridkin SK. 2014. Multistate point-prevalence survey of health care–associated infections. *N Engl J Med* 370:1198-1208.

5. Reynolds D, Kollef M. 2021. The epidemiology and pathogenesis and treatment of *Pseudomonas aeruginosa* infections: An update. *Drugs* 81:2117-2131

6. Cabrera-Aguas M, Khoo P, Watson SL. 2022. Infectious keratitis: A review. *Clin Exp Ophthalmol* 50:543-562

7. Ung L, Bispo PJM, Shanbhag SS, Gilmore MS, Chodosh J. 2019. The persistent dilemma of microbial keratitis: Global burden, diagnosis, and antimicrobial resistance. *Surv Ophthalmol* 64:255-271.

8. Collier SA, Gronostaj MP, MacGurn AK, Cope JR, Awsumb KL, Yoder JS, Beach MJ.

2014. Estimated burden of keratitis--United States, 2010. *MMWR* 63:1027–1030.

9. Stapleton F, Keay L, Edwards K, Naduvilath T, Dart JKG, Brian G, Holden BA. 2008. The incidence of contact lens-related microbial keratitis in Australia. *Ophthalmology* 115:1655–1662.

10. Durand ML, Barshak MB, Chodosh J. 2021. Infectious keratitis in 2021. *JAMA* 326:1319-1320

11. Morelli MK, Kloosterboer A, Fulton SA, Furin J, Newman N, Omar AF, Rojas LJ, Marshall SH, Yasmin M, Bonomo RA. 2023. Investigating and treating a corneal ulcer due to extensively drug-resistant *Pseudomonas aeruginosa*. *Antimicrob Agents Chemother* 67:e0027723.

12. Velcani F, Kuo IC, Shanks RMQ, Chodosh J, Garg P, Amescua G, Zegans ME. 2023. Association of artificial tears with ocular and systemic infection: Carbapenem-resistant *Pseudomonas aeruginosa* (VIM-GES-CRPA) Outbreak. *Ophthalmology* 130:1118-1120

13. Tribin FE, Lieux C, Maestre-Mesa J, Durkee H, Krishna K, Chou B, Neag E, Tothova JD, Martinez JD, Flynn Jr HW, Parel JM, Miller D, Amescua G. 2024. Clinical features and treatment outcomes of carbapenem-resistant *Pseudomonas aeruginosa* keratitis. *JAMA Ophthalmol* 142:407–415.

14. Lee EJ, Cowell BA, Evans DJ, Fleiszig SMJ. 2003. Contribution of ExsA-regulated factors to corneal infection by cytotoxic and invasive *Pseudomonas aeruginosa* in a murine scarification model. *Invest Ophthalmol Vis Sci* 44:3892–3898.

15. Tam C, Lewis SE, Li WY, Lee E, Evans DJ, Fleiszig SMJ. 2007. Mutation of the phospholipase catalytic domain of the *Pseudomonas aeruginosa* cytotoxin ExoU abolishes colonization promoting activity and reduces corneal disease severity. *Exp Eye Res* 85:799–

805.

16. Zolfaghar I, Evans DJ, Ronaghi R, Fleiszig SMJ. 2006. Type III secretion-dependent modulation of innate immunity as one of multiple factors regulated by *Pseudomonas aeruginosa* RetS. *Infect Immun* 74:3880–3889.

17. Zolfaghar I, Angus AA, Kang PJ, To A, Evans DJ, Fleiszig SMJ. 2005. Mutation of *retS*, encoding a putative hybrid two-component regulatory protein in *Pseudomonas aeruginosa*, attenuates multiple virulence mechanisms. *Microbes Infect* 7:1305-1316

18. Vance RE, Rietsch A, Mekalanos JJ. 2005. Role of the type III secreted exoenzymes S, T, and Y in systemic spread of *Pseudomonas aeruginosa* PAO1 *in vivo*. *Infect Immun* 73:1706–1713.

19. Shaver CM, Hauser AR. 2004. Relative contributions of *Pseudomonas aeruginosa* ExoU, ExoS, and ExoT to virulence in the lung. *Infect Immun* 72:6969–6977.

20. Goodman AL, Kulasekara B, Rietsch A, Boyd D, Smith RS, Lory S. 2004. A signaling network reciprocally regulates genes associated with acute infection and chronic persistence in *Pseudomonas aeruginosa*. *Dev Cell* 7:745–754.

21. Mekonnen SA, Husseini N El, Turdiev A, Carter JA, Belew AT, El-Sayed NM, Lee VT. 2022. Catheter-associated urinary tract infection by *Pseudomonas aeruginosa* progresses through acute and chronic phases of infection. *Proc Natl Acad Sci U S A* 119: e2209383119.

22. Rangel SM, Diaz MH, Knoten CA, Zhang A, Hauser AR. 2015. The role of ExoS in dissemination of *Pseudomonas aeruginosa* during pneumonia. *PLoS Pathog* 11:e1004945.

23. Hauser AR. 2009. The type III secretion system of *Pseudomonas aeruginosa*: infection by injection. *Nat Rev Microbiol* 7:654-665.

24. Angus AA, Lee AA, Augustin DK, Lee EJ, Evans DJ, Fleiszig SMJ. 2008. *Pseudomonas*

aeruginosa induces membrane blebs in epithelial cells, which are utilized as a niche for intracellular replication and motility. *Infect Immun* 76: 1992-2001.

25. Angus AA, Evans DJ, Barbieri JT, Fleiszig SMJ. 2010. The ADP-ribosylation domain of *Pseudomonas aeruginosa* ExoS is required for membrane bleb niche formation and bacterial survival within epithelial cells. *Infect Immun* 78:4500-4510.

26. Kroken AR, Chen CK, Evans DJ, Yahr TL, Fleiszig SMJJ. 2018. The impact of ExoS on *Pseudomonas aeruginosa* internalization by epithelial cells is independent of *fleQ* and correlates with bistability of type three secretion system gene expression. *MBio* 9:e00668-18.

27. Kroken AR, Gajenthra Kumar N, Yahr TL, Smith BE, Nieto V, Horneman H, Evans DJ, Fleiszig SMJ. 2022. Exotoxin S secreted by internalized *Pseudomonas aeruginosa* delays lytic host cell death. *PLoS Pathog* 18:e1010306.

28. Metruccio MME, Tam C, Evans DJ, Xie AL, Stern ME, Fleiszig SMJ. 2017. Contributions of MyD88-dependent receptors and CD11c-positive cells to corneal epithelial barrier function against *Pseudomonas aeruginosa*. *Sci Rep* 7:13829.

29. Augustin DK, Heimer SR, Tam C, Li WY, Le Due JM, Evans DJ, Fleiszig SMJ. 2011. Role of defensins in corneal epithelial barrier function against *Pseudomonas aeruginosa* traversal. *Infect Immun* 79:595-605.

30. Fleiszig SMJ, Kroken AR, Nieto V, Grosser MR, Wan SJ, Metruccio MME, Evans DJ. 2019. Contact lens-related corneal infection: Intrinsic resistance and its compromise. *Prog Retin Eye Res* 76: 100804.

31. Reins RY, Courson J, Lema C, Redfern RL. 2017. MyD88 contribution to ocular surface homeostasis. *PLoS One* 12:0182153.

32. Wan S, Datta A, Flandrin O, Metruccio MME, Ma S, Nieto V, Kroken AR, Hill RZ, Bautista DM, Evans DJ, Fleiszig SMJ. 2021. Nerve-associated transient receptor potential ion channels can contribute to intrinsic resistance to bacterial adhesion in vivo. *FASEB J* 35:e21899.

33. Tam C, Mun JJ, Evans DJ, Fleiszig SMJ. 2012. Cytokeratins mediate epithelial innate defense through their antimicrobial properties. *J Clin Invest* 122:3665-3677.

34. Mantelli F, Mauris J, Argüeso P. 2013. The ocular surface epithelial barrier and other mechanisms of mucosal protection: from allergy to infectious diseases. *Curr Opin Allergy Clin Immunol* 13:563-8.

35. Wan SJ, Sullivan AB, Shieh P, Metruccio MME, Evans DJ, Bertozzi CR, Fleiszig SMJ. 2018. IL-1R and MyD88 contribute to the absence of a bacterial microbiome on the healthy murine cornea. *Front Microbiol* 9:1117.

36. Wan SJ, Ma S, Evans DJ, Fleiszig SMJ. 2020. Resistance of the murine cornea to bacterial colonization during experimental dry eye. *PLoS One* 15:e0234013.

37. Alarcon I, Tam C, Mun JJJ, LeDue J, Evans DJ, Fleiszig SMJ. 2011. Factors impacting corneal epithelial barrier function against *Pseudomonas aeruginosa* traversal. *Invest Ophthalmol Vis Sci* 52:1368-1377.

38. Lee EJ, Evans DJ, Fleiszig SMJ. 2003. Role of *Pseudomonas aeruginosa* ExsA in penetration through corneal epithelium in a novel *in vivo* model. *Investig Ophthalmol Vis Sci* 44:5220-5227.

39. Kwong MSF, Evans DJ, Ni M, Cowell BA, Fleiszig SMJ. 2007. Human tear fluid protects against *Pseudomonas aeruginosa* keratitis in a murine experimental model. *Infect Immun* 75:2325-2332.

733 40. Fleiszig SMJ, Evans DJ, Do N, Vallas V, Shin S, Mostov KE. 1997. Epithelial cell polarity
734 affects susceptibility to *Pseudomonas aeruginosa* invasion and cytotoxicity. *Infect Immun*
735 65: 2861-2867.
736 41. Alarcon I, Kwan L, Yu C, Evans DJ, Fleiszig SMJ. 2009. Role of the corneal epithelial
737 basement membrane in ocular defense against *Pseudomonas aeruginosa*. *Infect Immun*
738 77:3264-3271.
739 42. Marquart ME. 2011. Animal models of bacterial Keratitis. *J Biomed Biotechnol*
740 2011:680642.
741 43. Hazlett LD. 2004. Corneal response to *Pseudomonas aeruginosa* infection. *Prog Retin Eye*
742 *Res* 23:1-30.
743 44. Tam C, Mun JJ, Evans DJ, Fleiszig SMJ. 2010. The impact of inoculation parameters on
744 the pathogenesis of contact lens-related infectious keratitis. *Invest Ophthalmol Vis Sci*
745 51:3100-3106.
746 45. Metruccio MME, Wan SJ, Horneman H, Kroken AR, Sullivan AB, Truong TN, Mun JJ,
747 Tam CKP, Frith R, Welsh L, George MD, Morris CA, Evans DJ, Fleiszig SMJ. 2019. A
748 novel murine model for contact lens wear reveals clandestine IL-1R dependent corneal
749 parainflammation and susceptibility to microbial keratitis upon inoculation with
750 *Pseudomonas aeruginosa*. *Ocul Surf* 17:119-133.
751 46. Azghani AO, Gray LD, Johnson AR. 1993. A bacterial protease perturbs the paracellular
752 barrier function of transporting epithelial monolayers in culture. *Infect Immun* 61:2681-
753 2686.
754 47. Azghani AO. 1996. *Pseudomonas aeruginosa* and epithelial permeability: role of virulence
755 factors elastase and exotoxin A. *Am J Respir Cell Mol Biol* 15:132-140.

48. Heiniger RW, Winther-Larsen HC, Pickles RJ, Koomey M, Wolfgang MC. 2010. Infection of human mucosal tissue by *Pseudomonas aeruginosa* requires sequential and mutually dependent virulence factors and a novel pilus-associated adhesin. *Cell Microbiol* 12:1158-73.

49. Golovkine G, Faudry E, Bouillot S, Elsen S, Attrée I, Huber P. 2016. *Pseudomonas aeruginosa* transmigrates at epithelial cell-cell junctions, exploiting sites of cell division and senescent cell extrusion. *PLoS Pathog* 12:e1005377.

50. Nomura K, Obata K, Keira T, Miyata R, Hirakawa S, Takano K ichi, Kohno T, Sawada N, Himi T, Kojima T. 2014. *Pseudomonas aeruginosa* elastase causes transient disruption of tight junctions and downregulation of PAR-2 in human nasal epithelial cells. *Respir Res* 15:21.

51. Alarcon I, Evans DJ, Fleiszig SMJ. 2009. The role of twitching motility in *Pseudomonas aeruginosa* exit from and translocation of corneal epithelial cells. *Invest Ophthalmol Vis Sci* 50:2237-2244.

52. Ramirez JC, Fleiszig SMJ, Sullivan AB, Tam C, Borazjani R, Evans DJ. 2012. Traversal of multilayered corneal epithelia by cytotoxic *Pseudomonas aeruginosa* requires the phospholipase domain of *exoU*. *Invest Ophthalmol Vis Sci* 53:448-453.

53. Leoni Swart A, Laventie B-J, Sütterlin R, Junne T, Lauer L, Manfredi P, Jakonia S, Yu X, Karagkiozi E, Okujava R, Jenal U. 2024. *Pseudomonas aeruginosa* breaches respiratory epithelia through goblet cell invasion in a microtissue model. *Nat Microbiol* 9:1725-1737.

54. Li J, Metruccio MME, Evans DJ, Fleiszig SMJ. 2017. Mucosal fluid glycoprotein DMBT1 suppresses twitching motility and virulence of the opportunistic pathogen *Pseudomonas aeruginosa*. *PLoS Pathog* 13:e1006392

779 55. Fleiszig SM, Zaidi TS, Ramphal R, Pier GB. 1994. Modulation of *Pseudomonas aeruginosa*
780 adherence to the corneal surface by mucus. *Infect Immun* 62:1799-1804.
781 56. Fleiszig SMJ, Kwong MSF, Evans DJ. 2003. Modification of *Pseudomonas aeruginosa*
782 interactions with corneal epithelial cells by human tear fluid. *Infect Immun* 71:3866-3874.
783 57. Mun JJ, Tam C, Evans DJ, Fleiszig SMJ. 2011. Modulation of epithelial immunity by
784 mucosal fluid. *Sci Rep* 1:8.
785 58. Tabor LM, Grosser MR, Metruccio MMME, Kumar NG, Wu YT, Nieto V, Evans DJ,
786 Fleiszig SMJ. 2021. Human tear fluid modulates the *Pseudomonas aeruginosa*
787 transcriptome to alter antibiotic susceptibility. *Ocul Surf* 22: 94-102.
788 59. Gao N, Lee P, Yu FS. 2016. Intraepithelial dendritic cells and sensory nerves are structurally
789 associated and functional interdependent in the cornea. *Sci Rep* 6: 36414
790 60. Jiao H, Ivanusic JJ, McMenamin PG, Chinnery HR. 2021. Distribution of corneal TRPV1
791 and its association with immune cells during homeostasis and injury. *Investig Opthalmology*
792 *Vis Sci* 62:6.
793 61. Downie LE, Zhang X, Wu M, Karunaratne S, Loi JK, Senthil K, Arshad S, Bertram K,
794 Cunningham AL, Carnt N, Mueller SN, Chinnery HR. 2023. Redefining the human corneal
795 immune compartment using dynamic intravital imaging. *Proc Natl Acad Sci U S A* 120:
796 e2217795120.
797 62. Sullivan AB, Tam KPC, Metruccio MME, Evans DJ, Fleiszig SMJ. 2015. The importance
798 of the *Pseudomonas aeruginosa* type III secretion system in epithelium traversal depends
799 upon conditions of host susceptibility. *Infect Immun* 83:1629-1640
800 63. McCaw ML, Lykken GL, Singh PK, Yahr TL. 2002. ExsD is a negative regulator of the
801 *Pseudomonas aeruginosa* type III secretion regulon. *Mol Microbiol* 46:1123-1133.

64. Rietsch A, Vallet-Gely I, Dove SL, Mekalanos JJ. 2005. ExsE, a secreted regulator of type III secretion genes in *Pseudomonas aeruginosa*. *Proc Natl Acad Sci U S A* 102:8006-8011.

65. Soong G, Parker D, Magargee M, Prince AS. 2008. The type III toxins of *Pseudomonas aeruginosa* disrupt epithelial barrier function. *J Bacteriol* 190:2814-2821.

66. Toska J, Sun Y, Carbonell DA, Foster ANS, Jacobs MR, Pearlman E, Rietsch A. 2014. Diversity of virulence phenotypes among type III secretion negative *Pseudomonas aeruginosa* clinical isolates. *PLoS One* 9:e86829.

67. Turnbull L, Toyofuku M, Hynen AL, Kurosawa M, Pessi G, Petty NK, Osvath SR, Cárcamo-Oyarce G, Gloag ES, Shimoni R, Omasits U, Ito S, Yap X, Monahan LG, Cavaliere R, Ahrens CH, Charles IG, Nomura N, Eberl L, Whitchurch CB. 2016. Explosive cell lysis as a mechanism for the biogenesis of bacterial membrane vesicles and biofilms. *Nat Commun* 7:11220.

68. Gonzalez D, Mavridou DAI. 2019. Making the best of aggression: The many dimensions of bacterial toxin regulation. *Trends Microbiol* 27:897-905.

69. Wydau-Dematteis S, El Meouche I, Courtin P, Hamiot A, Lai-Kuen R, Saubaméa B, Fenaille F, Butel MJ, Pons JL, Dupuy B, Chapot-Chartier MP, Peltier J. 2018. Cwp19 is a novel lytic transglycosylase involved in stationary-phase autolysis resulting in toxin release in clostridium difficile. *MBio* 9:e00648.

70. Redfern RL, Reins RY, McDermott AM. 2011. Toll-like receptor activation modulates antimicrobial peptide expression by ocular surface cells. *Exp Eye Res* 92:209-220.

71. Bai J, Kim SI, Ryu S, Yoon H. 2014. Identification and characterization of outer membrane vesicle-associated proteins in *Salmonella enterica* serovar Typhimurium. *Infect Immun* 82:4001-4010.

825 72. Kim SI, Kim S, Kim E, Hwang SY, Yoon H. 2018. Secretion of *Salmonella* pathogenicity
826 I island 1-encoded type III secretion system effectors by outer membrane vesicles in
827 *Salmonella enterica* Serovar Typhimurium. *Front Microbiol* 9:2810.
828 73. Sirisaengtaksin N, O'Donoghue EJ, Jabbari S, Roe AJ, Krachler AM. 2023. Bacterial outer
829 membrane vesicles provide an alternative pathway for trafficking of *Escherichia coli* O157
830 type III secreted effectors to epithelial cells. *mSphere* 8:e0052023
831 74. Metruccio MME, Evans DJ, Gabriel MM, Kadurugamuwa JL, Fleiszig SMJ. 2016.
832 *Pseudomonas aeruginosa* outer membrane vesicles triggered by human mucosal fluid and
833 lysozyme can prime host tissue surfaces for bacterial adhesion. *Front Microbiol* 7:1-19.
834 75. Hritonenko V, Evans DJ, Fleiszig SMJ. 2012. Translocon-independent intracellular
835 replication by *Pseudomonas aeruginosa* requires the ADP-ribosylation domain of ExoS.
836 *Microbes Infect* 14:1366-1373.
837 76. Heimer SR, Evans DJ, Stern ME, Barbieri JT, Yahr T, Fleiszig SMJ. 2013. *Pseudomonas*
838 *aeruginosa* utilizes the type III secreted toxin ExoS to avoid acidified compartments within
839 epithelial cells. *PLoS One* 8:e73111.
840 77. Kumar NG, Nieto V, Kroken AR, Jedel E, Grosser MR, Hallsten ME, Mettrucio MME,
841 Yahr TL, Evans DJ, Fleiszig SMJ. 2022. *Pseudomonas aeruginosa* can diversify after host
842 cell invasion to establish multiple intracellular niches. *mBio* 13:e0274222
843 78. Kroken AR, Klein KA, Mitchell PS, Nieto V, Jedel EJ, Evans DJ, Fleiszig SMJ. 2023.
844 Intracellular replication of *Pseudomonas aeruginosa* in epithelial cells requires suppression
845 of the caspase-4 inflammasome. mSphere 8:e00351.
846 79. Epelman S, Stack D, Bell C, Wong E, Neely GG, Krutzik S, Miyake K, Kubes P, Zbytnuik
847 LD, Ma LL, Xie X, Woods DE, Mody CH. 2004. Different domains of *Pseudomonas*

aeruginosa exoenzyme S activate distinct TLRs . *J Immunol* 173:2031-2040.

80. Epelman S, Neely GG, Ma LL, Gjomarkaj M, Pace E, Melis M, Woods DE, Mody CH. 2002. Distinct fates of monocytes and T cells directly activated by *Pseudomonas aeruginosa* exoenzyme S . *J Leukoc Biol* 71:458-68

81. Dortet L, Lombardi C, Cretin F, Dessen A, Filloux A. 2018. Pore-forming activity of the *Pseudomonas aeruginosa* type III secretion system translocon alters the host epigenome. *Nat Microbiol* 3:378-386.

82. Miao EA, Mao DP, Yudkovsky N, Bonneau R, Lorang CG, Warren SE, Leaf IA, Aderem A. 2010. Innate immune detection of the type III secretion apparatus through the NLRC4 inflammasome. *Proc Natl Acad Sci U S A* 107:3076-3080.

83. Rayamajhi M, Zak DE, Chavarria-Smith J, Vance RE, Miao EA. 2013. Cutting edge: Mouse NAIP1 detects the type III secretion system needle protein. *J Immunol* 191: 3986-3989

84. Mun JJ, Tam C, Kowbel D, Hawgood S, Barnett MJ, Evans DJ, Fleiszig SMJ. 2009. Clearance of *Pseudomonas aeruginosa* from a healthy ocular surface involves surfactant protein D and is compromised by bacterial elastase in a murine null-infection model. *Infect Immun* 77:2392-2398.

85. Rietsch A, Mekalanos JJ. 2006. Metabolic regulation of type III secretion gene expression in *Pseudomonas aeruginosa*. *Mol Microbiol* 59:807-820.

86. Sosnová-Netuková M, Kuchynka P, Forrester J V. 2007. The suprabasal layer of corneal epithelial cells represents the major barrier site to the passive movement of small molecules and trafficking leukocytes. *Br J Ophthalmol* 91:372-378.

87. MacDonald IA, Kuehna MJ. 2013. Stress-induced outer membrane vesicle production by *Pseudomonas aeruginosa*. *J Bacteriol* 195:2971-2981.

88. Simonis A, Kreer C, Albus A, Rox K, Yuan B, Holzmann D, Wilms JA, Zuber S, Kottege L, Winter S, Meyer M, Schmitt K, Gruell H, Theobald SJ, Hellmann AM, Meyer C, Ercanoglu MS, Cramer N, Munder A, Hallek M, Fätkenheuer G, Koch M, Seifert H, Rietschel E, Marlovits TC, van Koningsbruggen-Rietschel S, Klein F, Rybniker J. 2023. Discovery of highly neutralizing human antibodies targeting *Pseudomonas aeruginosa*. *Cell* 186:5098-5113

89. Goldberg JB, Crisan C V., Luu JM. 2022. *Pseudomonas aeruginosa* antivirulence strategies: Targeting the type III secretion system. *Adv Exp Med Biol* 1386:257-280

90. Hmelo LR, Borlee BR, Almblad H, Love ME, Randall TE, Tseng BS, Lin C, Irie Y, Storek KM, Yang JJ, Siehnel RJ, Howell PL, Singh PK, Tolker-Nielsen T, Parsek MR, Schweizer HP, Harrison JJ. 2015. Precision-engineering the *Pseudomonas aeruginosa* genome with two-step allelic exchange. *Nat Protoc* 10:1820-1841.

91. Choi KH, Schweizer HP. 2006. Mini-Tn7 insertion in bacteria with single attTn7 sites: Example *Pseudomonas aeruginosa*. *Nat Protoc* 1:153-161.

92. Tam C, LeDue J, Mun JJ, Herzmark P, Robey EA, Evans DJ, Fleiszig SMJ. 2011. 3D quantitative imaging of unprocessed live tissue reveals epithelial defense against bacterial adhesion and subsequent traversal requires MyD88. *PLoS One* 6:e24008.

93. Guthoff RF, Zhivov A, Stachs O. 2009. In vivo confocal microscopy, an inner vision of the cornea - A major review. *Clin Exp Ophthalmol* 37:100-117.

94. Bleves S, Soscia C, Nogueira-Orlandi P, Lazdunski A, Filloux A. 2005. Quorum sensing negatively controls type III secretion regulon expression in *Pseudomonas aeruginosa* PA

95. Cisz M, Lee PC, Rietsch A. 2008. ExoS controls the cell contact-mediated switch to effector secretion in *Pseudomonas aeruginosa*. *J Bacteriol* 190:2726-38

894 96. Bloemberg G V, O'Toole G a, Lugtenberg BJ, Kolter R. 1997. Green fluorescent protein as
895 a marker for *Pseudomonas* spp. *Appl Environ Microbiol* 63:4543-4551.
896 97. Brutinel ED, Vakulskas CA, Brady KM, Yahr TL. 2008. Characterization of ExsA and of
897 ExsA-dependent promoters required for expression of the *Pseudomonas aeruginosa* type
898 III secretion system. *Mol Microbiol* 68:657-671.
899

900 Table 1. Properties and epithelial traversal results for *P. aeruginosa PAO1F and T3SS mutants*

901

Strain	Exotoxins	Translocon	Needle	Epithelial Traversal
PAO1F	+	+	+	++
Δ*exsD*	++	++	++	+
Δ*pscC*	+	+	-	++
Δ*popBD*	+	-	+	+
Δ*exoSTY*	-	+	+	+
Δ*pscC*Δ*popBD*	+	-	-	++
Δ*popB*Δ*exoSTY*	-	-	+	-
Δ*pscU-L:P*$_{rha}$*exsA*	+	-	-	+
Δ*pscU-L*Δ*exoSTY:P*$_{rha}$*exsA*	-	-	-	-

902

903

904

905

906

907

908

909

910

911

912

913

914

915

916 Table 2. Strains, mutants, and plasmids used in this study

Strain or mutant	Description	Source
PAO1F	Wild-type *P. aeruginosa*; All mutants made within this background	Dr. Alain Filloux *via* Dr. Arne Rietsch (94)
Δ*exsA*	*exsA* mutant; Constitutively T3SS^{Off}	Dr. Arne Rietsch
Δ*exsD*	*exsD* mutant; Constitutively T3SS^{On}	Dr. Timothy Yahr (63)
Δ*pscC*	*pscC* mutant; Lacking needle	Dr. Arne Rietsch (95)
Δ*popBD*	*popBD* double mutant; Lacking translocon pore	Dr. Arne Rietsch (95)
Δ*exoSTY*	*exoSTY* triple mutant; Lacking known exotoxins	Dr. Arne Rietsch (95)
Δ*pscU-L*	Total T3SS-operon mutant (knockout of all genes *pscU* to *pscL*); called *ΔU-L*	Dr. Arne Rietsch (66)
Δ*exsA:Prha-A*	*exsA* mutant with chromosome-integrated rhamnose-inducible *exsA*	Dr. Abby Kroken (27)
Δ*pscU-L:Prha-A*	Δ*U-L* with rhamnose-inducible *exsA*	This study
Δ*pscU-L:Prha-V*	Δ*U-L* with rhamnose-inducible vector control	This study
Δ*pscU-L* Δ*exoSTY:Prha-A*	Δ*U-L* lacking all known exotoxins, with rhamnose-inducible *exsA*	This study
Δ*popB*Δ*exoSTY*	*popB* mutant lacking all known exotoxins	Dr. Victoria Hritonenko (75)
Δ*pscC*Δ*popBD*	*popBD* mutant lacking T3SS needle	This study
Δ*popB*Δ*exoS*	*popB* mutant lacking *exoS*	This study
E. coli SM10(λ*pir*)	Mutagenesis vector donor strain	New England Biolabs
Plasmid	**Description (Resistance conferred, µg/ml)**	**Source**
pSMC2	Constitutive GFP (Carbenicillin, 400)	(96)
pJNE05	T3SS-GFP (P*exoS*). Plasmid encoding *gfp* fused to the ExsA-dependent promoter of *exoS*. (Gentamicin, 200)	(97)
pEXG2-Δ*pscU-L*	Integrating suicide plasmid for mutagenesis	Dr. Arne Rietsch
pEXG2-Δ*exoS*	Integrating suicide plasmid for mutagenesis	Dr. Arne Rietsch
pUC18-mini-Tn7T-PrhaB-*exsA*	Delivery vector for integrating *exsA* under Rhamnose-sensitive promoter to *att*Tn7 site (Carbenicillin, 100)	This study
pUC18-mini-Tn7T-PrhaB-Vector	Delivery vector for integrating empty expression vector under rhamnose-sensitive promoter to *att*Tn7 site (Carbenicillin, 100)	This study
pTNS1	Helper plasmid for conjugation of Tn7 integration plasmid (Ampicillin, 100)	(91)
pRK2013	Helper plasmid for conjugation of Tn7 integration plasmid (Kanamycin, 35)	(91)
pFLP2	Sucrose-sensitive vector to excise antibiotic resistance marker from *att*Tn7 site	(91)

FIGURE LEGENDS

Figure 1. Method for quantitative imaging and analysis of bacterial traversal of the corneal epithelium. Whole murine eyeballs *ex vivo* were blotted with tissue paper, incubated in 0.1M EGTA solution (1 h), then infected with ~1 x 10^{11} CFU/ml *P. aeruginosa* expressing GFP. Eyes were fixed, whole mounted *en face*, and imaged by confocal microscopy. (A) Raw image imported into Imaris 9.9 for 3D analysis, confocal reflectance signal shown in red and bacterial fluorescence in green. (B) Boundary between stroma and epithelium manually delineated in sequential XZ slices to exclude signal from stroma and create epithelium object. (C) Objects representing apical and basal boundaries of epithelium. (D) Bacteria automatically identified by fluorescent signal quality. (E) Bacteria colored by their depth of traversal, measured as a percentage of its position from the apical to basal boundaries.

Figure 2. Epithelial traversal by wild-type or T3SS mutants. (A) Traversal depth after *ex vivo* infection by PAO1F and T3SS mutants in genes encoding the transcriptional activator *exsA*, transcriptional repressor *exsD*, known exotoxins *exoSTY*, needle component *pscC*, or translocon pore *popBD*. Each data point represents the relative position (% depth) of one bacterium between the apical and basal boundaries of the 3D corneal epithelium. All data points pooled from ≥ 4 eyes per group. Error bars show the median +/- interquartile range. Note: All comparisons between the T3SS mutants with the Δ*exsA* mutant were significant as were all comparisons with wild-type PAO1F ($P < 0.0001$, Kruskal-Wallis test with Dunn's multiple comparisons). (B) Cumulative histogram graphing traversal data (from Fig. 2A) of wild-type and T3SS mutants as a percent of the total bacterial population found deeper in the epithelium. The vertical line indicates halfway

through the epithelium, highlighting the proportion of each strain that traversed more than 50% of the epithelial layer.

Figure 3. ExsA complementation in a T3SS operon-deficient background. (A) Traversal depth after *ex vivo* infection by a Δ*pscU-L* mutant which lacks all T3SS genes except *exoSTY* (and their respective chaperones) and a Δ*pscU-L*Δ*exoSTY* mutant which also lacks effector toxins. Controls include expression of an empty vector or *exsA* induced by overnight growth on and inclusion of 2% rhamnose during infection. Data were pooled from ≥ 3 eyes per strain. Error bars show median +/- interquartile range. All comparisons between groups were significant at $P < 0.0001$ except for Δ*pscU-L* vs. Δ*pscU-L*Δ*exoSTY*:P_{rha}-*exsA* + rhamnose, which had $P = 0.025$ (Kruskal-Wallis test with Dunn's multiple comparisons). (B) Cumulative histogram graphing traversal data (from Fig. 3A) of T3SS operon-deficient mutants with ExsA complementation or controls as a percent of the total bacterial population found deeper in the epithelium. The vertical line indicates halfway through the epithelium, highlighting the proportion of each strain that traversed more than 50% of the epithelial layer.

Figure 4. Traversal by translocon and needle- or exotoxin-deficient mutants. (A) Traversal depth after *ex vivo* infection by T3SS translocon mutants in a background of Δ*pscC*, Δ*exoS*, or Δ*exoSTY*. Data from Fig. 2A was used for Δ*pscC* and Δ*exoSTY* mutants. Data pooled from ≥3 eyes per strain. Error bars show median +/- interquartile range. All comparisons between groups were significant ($P < 0.0001$, Kruskal-Wallis test with Dunn's multiple comparisons) except for Δ*exoSTY* vs. Δ*popB*. (B) Cumulative histogram graphing traversal data (from Fig. 4A) of the T3SS mutants as a percent of the total bacterial population found deeper in the epithelium. The vertical

963 line indicates halfway through the epithelium, highlighting the proportion of each strain that
964 traversed more than 50% of the epithelial layer.
965
966 **Figure 5. Rhamnose-induction of ExsA-driven ExoS expression in both bacterial cells and**
967 **supernatant of a needle-deficient mutant Δ*pscU-L*.** Western immunoblot showing bacterial cell
968 pellets and supernatant fractions collected from Δ*exsA*:P$_{rha}$*exsA*, Δ*pscU-L*:P$_{rha}$Vector, Δ*pscU-*
969 *L*:P$_{rha}$*exsA* after growth to 'mid-log' phase in LB media, with induction of *exsA* by 2% rhamnose
970 inclusion for the conditions indicated. The location of bands corresponding with ExoS (~49 kDa)
971 detected by affinity-purified antibody and chemiluminescence are evident below the protein
972 standard annotated at 50 kDa.
973
974 **Supplemental Material**
975
976 **Supplemental Figure S1. Comparison of corneal epithelium traversal by *P. aeruginosa* and**
977 **its T3SS mutants.** Representative images of corneal epithelium traversal by wild-type PAO1F
978 compared to the Δ*pscC*, Δ*popBD* and Δ*exoSTY* mutants color-coded for traversal depth.
979
980 **Supplemental Figure S2. EGTA induction of *P. aeruginosa* T3SS gene expression was similar**
981 **between PAO1 and T3SS mutants.** OD_{600}-normalized GFP signal from pJNE05 (P*exoS*) carried
982 by PAO1F or its T3SS mutants in the translocon pore Δ*popBD*, known exotoxins Δ*exoSTY*, or the
983 transcriptional repressor Δ*exsD* after 24 h growth in T3SS-induction media [TSB plus gentamicin
984 (200 μg/ml), monosodium glutamate (100 mM), glycerol (1 %) and EGTA (2 mM)]. Similar P*exoS*
985 induction, i.e. T3SS induction, was observed across wild-type and mutants. N = 3 separate growth

curves per group. Mean +/- standard deviation, ns = not significant (One-way ANOVA with Dunnett's Multiple Comparisons).

Supplemental Figure S3. Rhamnose-induction of ExsA rescues *ex vivo* traversal. (A) OD_{600}-normalized GFP signal from pJNE05 (P*exoS*) carried by a Δ*exsA* mutant complemented with rhamnose-inducible *exsA* with or without inclusion of rhamnose (Rha) (2 %) in the growth medium [TSB with gentamicin (200 μg/ml), monosodium glutamate (100 mM) and glycerol (1%)] after 24 h of growth. N = 3 separate growth curves per group. Mean +/- standard deviation, ** $P < 0.01$ (Paired Student's t-Test). (B) Traversal depth after *ex vivo* infection of Δ*exsA* with expression of *exsA* remaining off or induced by overnight growth with rhamnose (2 %). Data pooled from 3 eyes per strain. Error bars show the median with interquartile range. **** $P < 0.0001$ (Kolmogorov-Smirnov test).

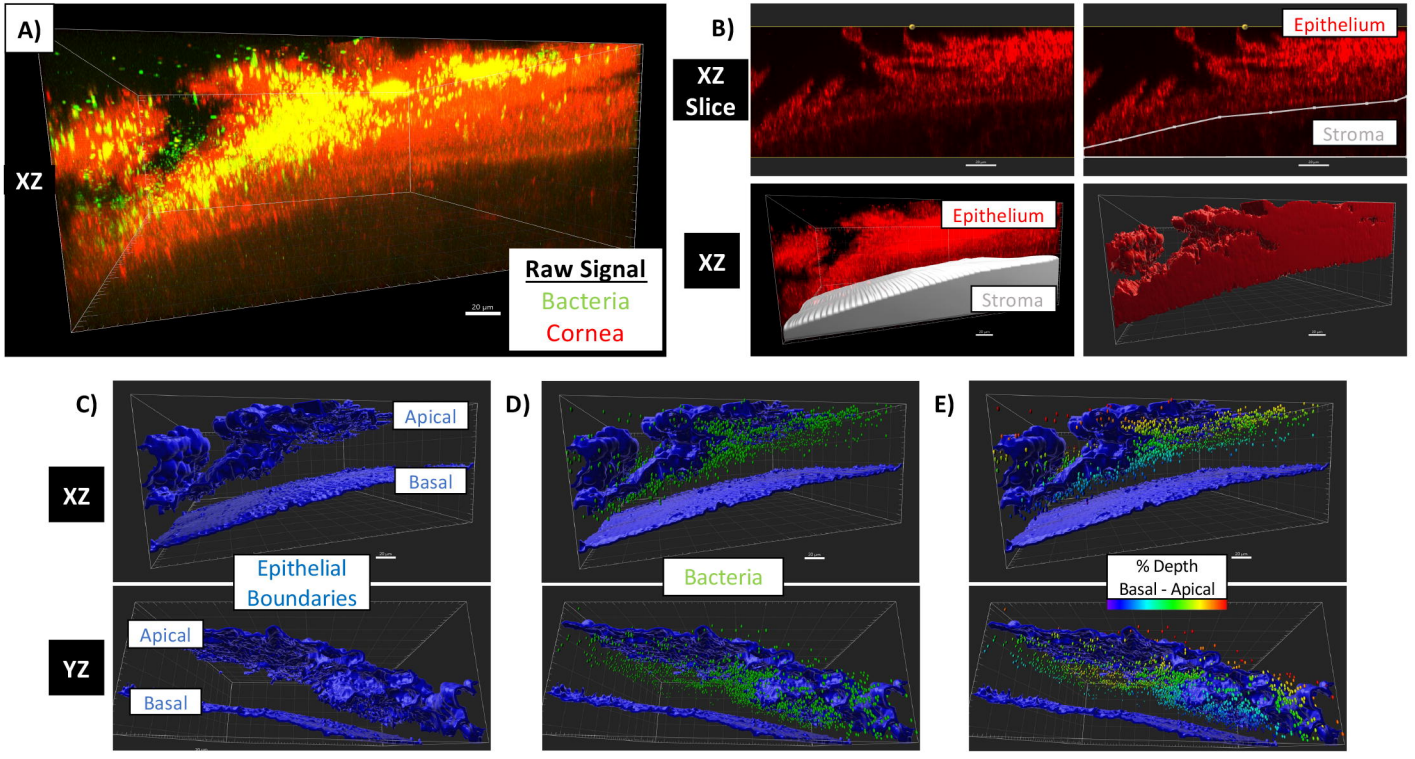
A)
XZ
Raw Signal
Bacteria
Cornea
20 µm
B)
XZ Slice
Epithelium
Stroma
XZ
Epithelium
Stroma
C)
XZ
Apical
Basal
Epithelial Boundaries
YZ
Apical
Basal
D)
Bacteria
E)
% Depth
Basal - Apical

A)

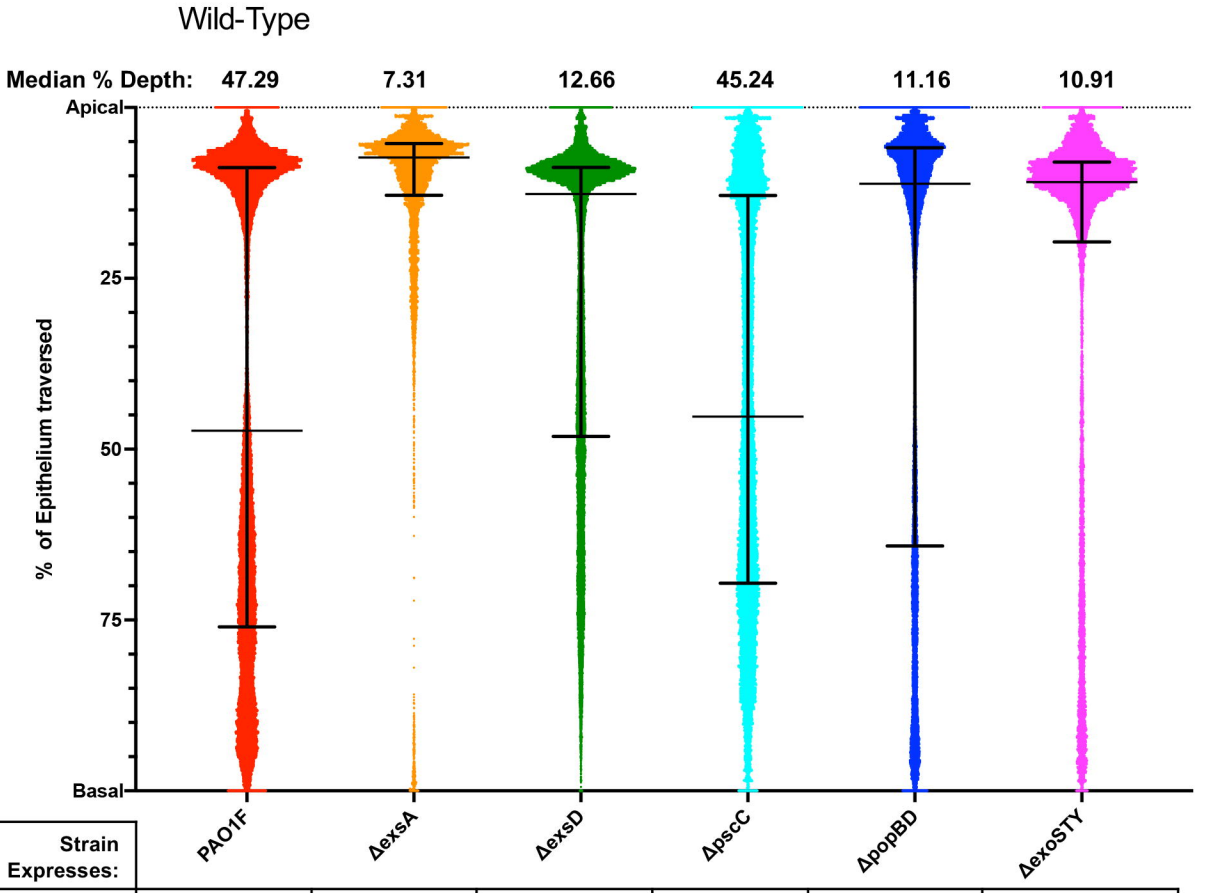

Strain Expresses:	PAO1F	ΔexsA	ΔexsD	ΔpscC	ΔpopBD	ΔexoSTY
ExsA	+	–	+	+	+	+
Needle	+	–	+	–	+	+
Translocon	+	–	+	+	–	+
Effectors	+	–	+	+	+	–

B)

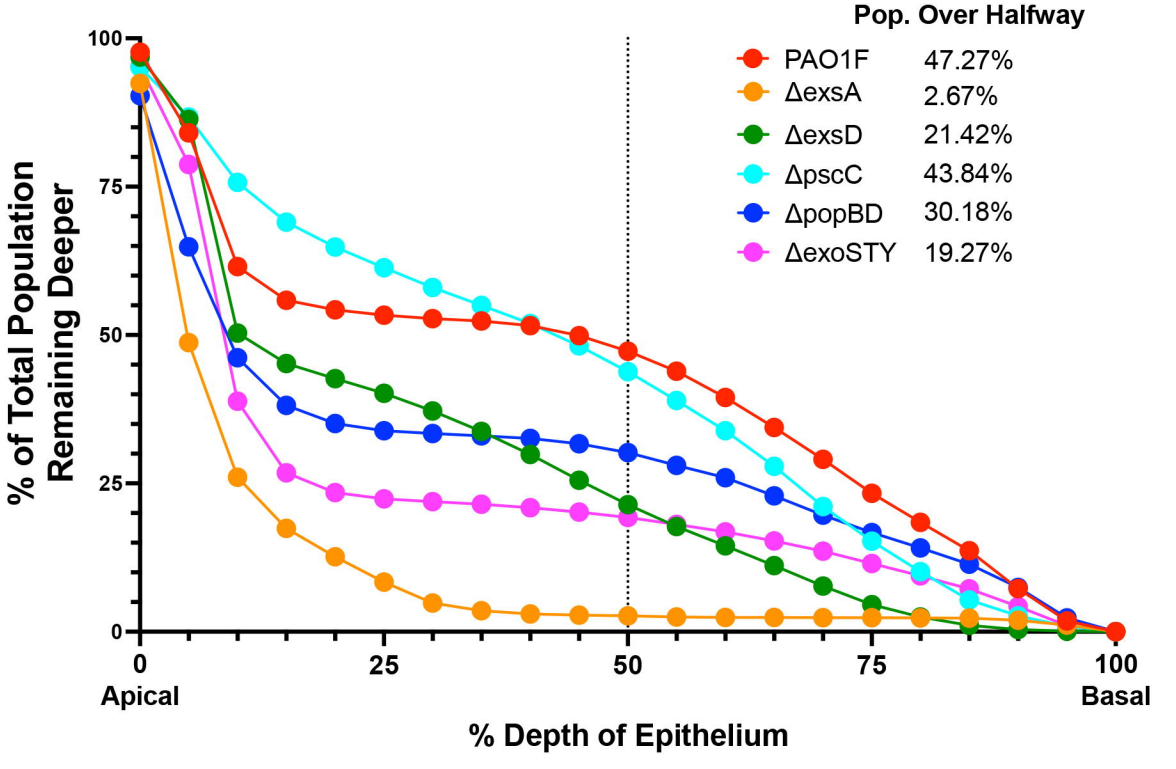

A)

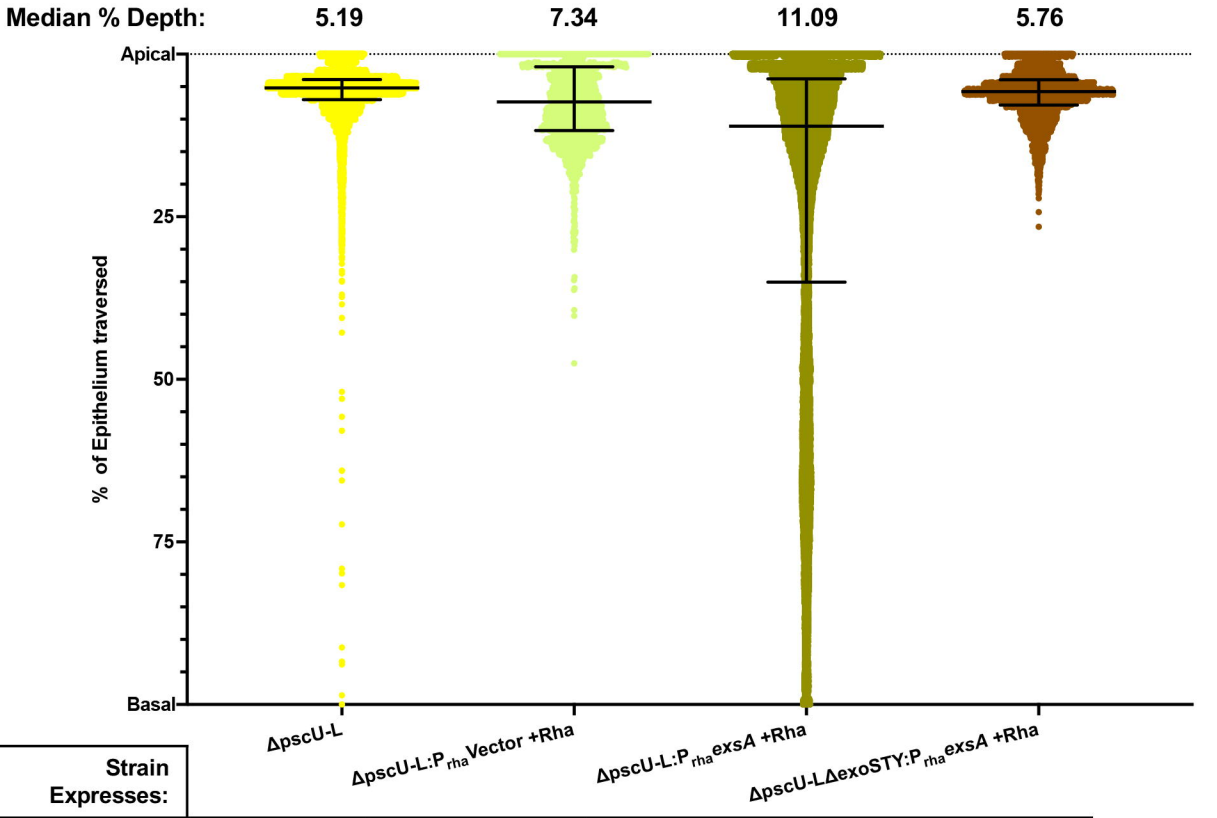

Strain Expresses:				
ExsA	–	–	+	+
Needle	–	–	–	–
Translocon	–	–	–	–
Effectors	–	–	+	–

B)

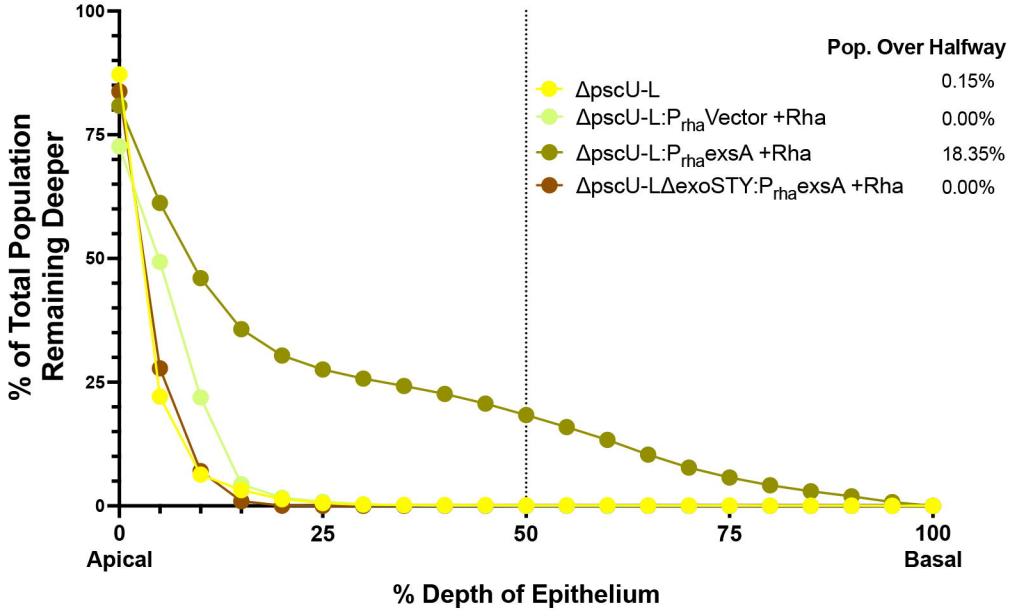

A)

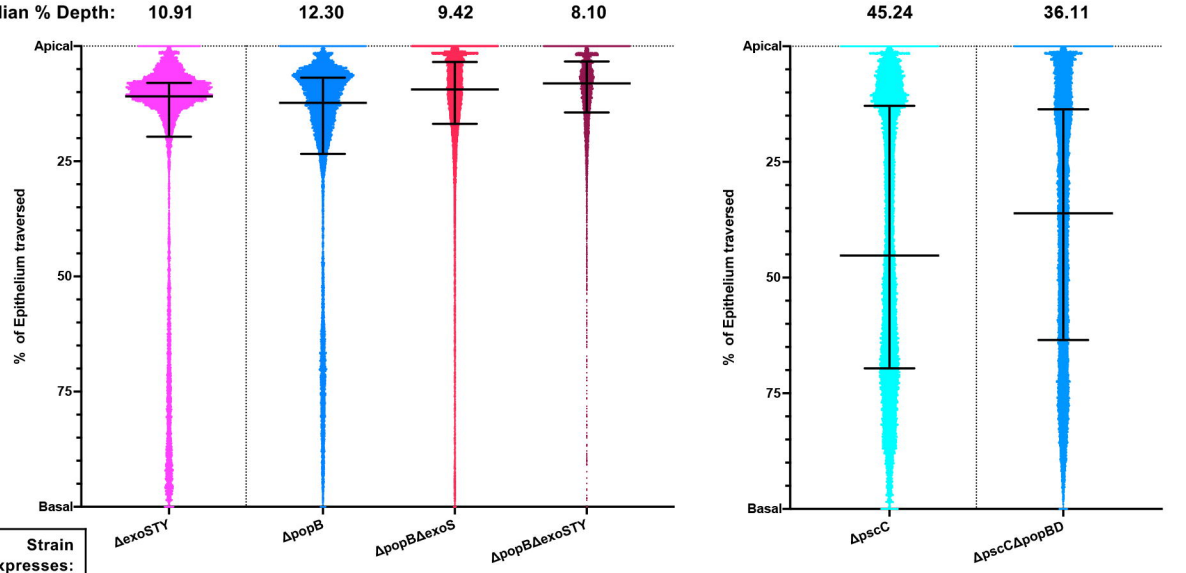

Strain Expresses:	ΔexoSTY	ΔpopB	ΔpopBΔexoS	ΔpopBΔexoSTY	ΔpscC	ΔpscCΔpopBD
ExsA	+	+	+	+	+	+
Needle	+	+	+	+	–	–
Translocon	+	–	–	–	+	–
Effectors	–	+	only *exoTY*	–	+	+

B)

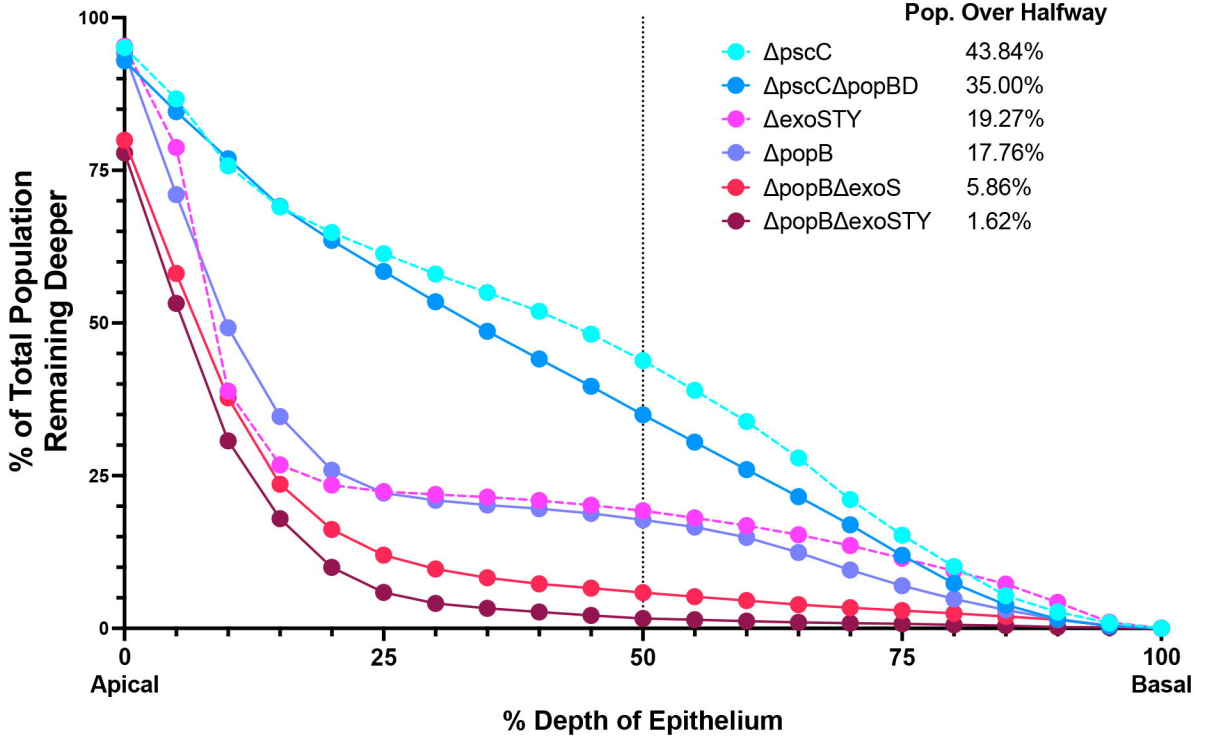

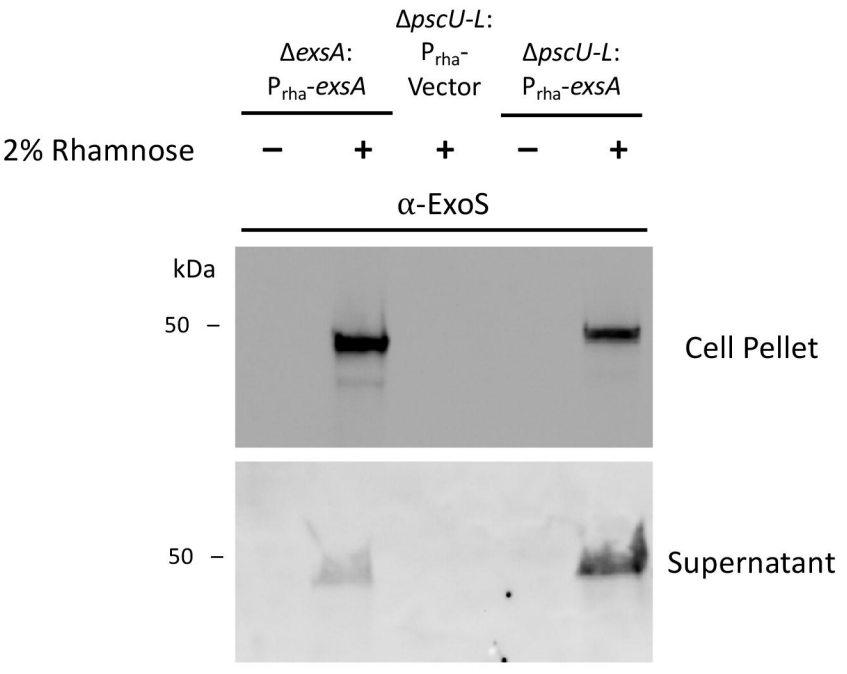
ΔexsA: Prha-exsA
ΔpscU-L: Prha-Vector
ΔpscU-L: Prha-exsA
2% Rhamnose
− + + − +
α-ExoS
kDa
50 –
Cell Pellet
50 –
Supernatant